

Projeto de Graduação



July 22, 2018

## **Power Amplifier for Inductive Wireless Power Transmission System**

Victoria Menescal Tupper Palhares



[www.ele.puc-rio.br](http://www.ele.puc-rio.br)



## **Power Amplifier for Inductive Wireless Power Transmission System**

**Student: Victoria Menescal Tupper Palhares**

**Advisor: Gláucio Lima Siqueira**

**Co-advisors: Jorge Mitrione**

Work presented as partial requirement to the conclusion of the Bacharelado em Engenharia Elétrica in the Pontifícia Universidade Católica do Rio de Janeiro, Rio de Janeiro, Brazil.

## Acknowledgements

I would first like to thank my mother, who taught me the significance of perseverance and hard work. Without her I would never be pursuing this path. I would also like to thank my father for teaching me how important it is to do what you love. Next, I would like to thank Alexandra, Gabriel and Patricia who always prayed for my success and supported me in moments of need.

I would like to thank my advisors, Prof. Gláucio Siqueira and Prof. Marbey Mosso, for giving me this opportunity and for always believing in my potential. I would also like to thank the Metamaterials Brazilian Society (SBMETA), for introducing me to this exciting topic and giving me guidance in this work.

I would like to thank my co-advisor, Jorge Mitrione, Ph.D., for his daily support at the Microwave Laboratory and for never giving up on this project or me.

I would like to thank my other co-advisor, Jorge Virgilio, M.Sc.Eng, who is the very reason of why I am here and the greatest enthusiastic of this project.

I would like to thank the Universidade Federal Fluminense (UFF), specially Prof. Vanessa Magri, for her amazing support and generosity in this project.

I would like to thank my, not only professors but also friends, Prof. Ana Pavani and Prof. Guilherme Temporão, who have been accompanying me throughout this entire journey and giving me unconditional support.

I would like to thank my classmates, Riobotz, my friends from the US and everyone who helped me overcome this challenge.

## Abstract

Over the last decades, dealing with batteries and wires has been a real challenge to industry. Many have been looking to alternatives such as non-radiative wireless power transmission (WPT) in order to give autonomy to devices. Non-radiative methods, in particular inductive coupling, has attracted a lot of attention because it is human safe and environmentally friendly. The drawback with this technology is the operating range which is very limited seeing it is a near field technique. In [1] it is presented a solution to improve the effective distance of an inductive coupling based WPT system using metamaterials (MTM). In the present work, a power amplifier (PA) was designed, fabricated and tested in order to improve previous performances. Simulations and experiments of the proposed PA are presented. The improvement of inductive power transmission (IPT) efficiency is supported by empirical evidences. This work is written integrally in the English language.

**Keywords: Power Amplifiers, Wireless Power Transmission, Inductive Coupling, Metamaterials**

# **Amplificador de Potência para Sistema de Transmissão de Potência Sem Fio por Indução**

## **Resumo**

Nas últimas décadas, lidar com baterias e fios têm sido um verdadeiro desafio para a indústria. Para dar autonomia aos dispositivos, muitos têm olhado para alternativas em transmissão de potência sem fio não radiativa. Métodos não radiativos, especialmente acoplamento indutivo, têm atraído muita atenção pelo fato de não afetarem a saúde dos seres humanos e serem sustentáveis. Entretanto, é inconveniente devido ao seu limitado raio de operação, considerando que é uma técnica para campo próximo. Em [1], é apresentada uma solução para a melhoria da distância efetiva de um sistema de transmissão de energia sem fio baseado em acoplamento indutivo, utilizando metamateriais. No presente trabalho, um amplificador de potência foi projetado, fabricado e testado para melhorar as performances anteriores. Simulações e experimentos deste proposto amplificador de potência estão presentes neste trabalho. O progresso na eficiência da transmissão indutiva de energia foi provado por evidências empíricas. Este trabalho está inteiramente escrito na Língua Inglesa.

**Palavras-chave: Amplificadores de Potência, Transmissão de Energia sem Fio, Acoplamento Indutivo, Metamateriais**

## List of Figures

1	Wardenclyffe Tower . . . . .	1
2	QSCR in the Disney Project. . . . .	2
3	Electric car being charged while moving in a highway. . . . .	2
4	Laser based system for WPT. [2] . . . . .	3
5	Space surrounding a small loop antenna . . . . .	6
6	Wave Impedance as a function of Distance [1] . . . . .	7
7	Electrical Transformer . . . . .	7
8	Devices that use inductive coupling . . . . .	8
9	Resonant Circuit . . . . .	9
10	Coupled Resonator System . . . . .	9
11	Qualcomm Halo Technology - Application of Magnetic Resonant Coupling . . . . .	10
12	Focalizing the far field (A) and the near field (B) [3] . . . . .	13
13	MSRR with N=4 [1] . . . . .	13
14	SR with N=12 [1] . . . . .	14
15	MTM for 13.56 MHz (front) . . . . .	16
16	MTM for 13.56 MHz (back) . . . . .	17
17	Lumped Capacitors connected in series with inductos via two holes. [1] . . . . .	17
18	MTM for 13.6 MHz (front) . . . . .	18
19	MTM for 33 MHz (back) . . . . .	19
20	Two types of BJT . . . . .	20
21	Operation Regions [4] . . . . .	21
22	Common Emitter Topology [4] . . . . .	22
23	Two types of BJT [4] . . . . .	22
24	Frequency Response of a topology with BJT [4] . . . . .	23
25	Output Waveform - Class A [4] . . . . .	24
26	Circuit Example - Class A [4] . . . . .	24
27	Transfer Function - Class A [4] . . . . .	24
28	Output Waveform - Class B [4] . . . . .	25
29	Circuit Example - Class B [4] . . . . .	25
30	Transfer Function - Class B [4] . . . . .	26
31	Output Waveform - Class AB [4] . . . . .	26
32	Circuit Example - Class AB [4] . . . . .	27
33	Transfer Function - Class AB [4] . . . . .	27
34	Transfer Function - Class C [5] . . . . .	28
35	Circuit Example - Class D [6] . . . . .	28

36	Circuit Example - Class E [6] . . . . .	29
37	Circuit Example - Class E [4] . . . . .	29
38	Low and Medium Power BJT [4] . . . . .	30
39	High Power [4] . . . . .	30
40	Comparison between DC component and the complete signal . . . . .	31
41	Transmission Line [7] . . . . .	31
42	Old Experiment . . . . .	33
43	Amplifying System . . . . .	33
44	First Schematic [8] . . . . .	34
45	Comparison between two substrates . . . . .	37
46	Final Layout for the MRF 426 in FR-4 . . . . .	37
47	Simulation Schematic in ADS . . . . .	38
48	Power from S21(Transmitted Power) . . . . .	38
49	Transmitted Power in dB . . . . .	39
50	LPKF ProtoMat S103 [9] . . . . .	40
51	Two Prototypes - With and without Ferric Chloride . . . . .	40
52	Final Circuit . . . . .	41
53	VNA . . . . .	42
54	PA Test . . . . .	43
55	Circuit Attenuators . . . . .	43
56	Output power when input power is -10 dBm and -5 dBm . . . . .	44
57	Output power when input power is -3 dBm and 0 dBm . . . . .	44
58	Output power when input power is 3 dBm and 5 dBm . . . . .	44
59	Output power when input power is 8 dBm and 10 dBm . . . . .	45
60	Output power when input power is 13 dBm and 16 dBm . . . . .	45
61	Experiment without MTMs . . . . .	46
62	Experiment with MTM 1 (13.6 MHz) . . . . .	47
63	Experiment with MTM 2 (33 MHz) . . . . .	47
64	Equipment used in the experiment . . . . .	47
65	Rectifier Circuit . . . . .	48
66	Experiment without MTMs . . . . .	49
67	Experiment with MTM 1 (13.6 MHz) . . . . .	49
68	Experiment with MTM 2 (33 MHz) . . . . .	49
69	20 dB Attenuator . . . . .	50
70	Without MTM . . . . .	50
71	One Slab of MTM 1 (13.6 MHz) assisting the Transmitter and the Receiver . . . . .	51
72	One Slab of MTM 2 (33 MHz) assisting the Transmitter and the Receiver . . . . .	51

73	Two experiments with MTM 1 (13.6 MHz) . . . . .	51
74	Two experiments with MTM 2 (33 MHz) . . . . .	52

## List of Tables

1	Region Separation . . . . .	5
2	Electromagnetically Small Antennas . . . . .	5
3	WPT Advantages and Drawbacks . . . . .	12
4	Types of MTMs . . . . .	12
5	Initial Model's Components . . . . .	35
6	Inductance Equivalency . . . . .	35
7	Results - PA Experiment . . . . .	46
8	LED Experiment . . . . .	48

## Acronyms

- ADS** Advanced Design System.
- BJT** Bipolar Junction Transistor.
- EM** Electromagnetic.
- IPT** Inductive Power Transmission.
- LED** Light Emitting Diode.
- LOS** Line of Sight.
- MSRR** Multiple Split Ring Resonator.
- MTM** Metamaterial.
- PA** Power Amplifier.
- PCB** Printed Circuit Board.
- PTE** Power Transfer Efficiency.
- QSCR** Quasistatic Cavity Resonance.
- RF** Radio Frequency.
- SR** Spiral Resonator.
- SRR** Split Ring Resonator.
- VNA** Vector Network Analyzer.
- VSWR** Voltage Stationary Wave Rate.
- WPC** Wireless Power Consortium.
- WPT** Wireless Power Transmission.

## Summary

<b>1. Introduction</b>	<b>1</b>
1.a. Historical Context . . . . .	1
1.b. State of the Art . . . . .	4
1.c. Objective . . . . .	4
1.d. Chapters Description . . . . .	4
<b>2. Theory</b>	<b>5</b>
2.a. Electromagnetic Theory . . . . .	5
2.a.1. Far Field vs. Near Field Regions . . . . .	5
2.a.2. Inductive Coupling . . . . .	7
2.a.3. Magnetic Resonant Coupling . . . . .	9
2.a.4. EM Radiation . . . . .	10
2.a.5. Overview . . . . .	12
2.b. Metamaterials . . . . .	12
2.b.1. Theory . . . . .	12
2.b.2. Models . . . . .	13
2.b.3. Design . . . . .	15
<b>3. Theory of Power Amplifiers</b>	<b>20</b>
3.a. Bipolar Junction Transistor (BJT) . . . . .	20
3.b. Classes of Amplifiers . . . . .	23
3.b.1. Class A . . . . .	23
3.b.2. Class B . . . . .	25
3.b.3. Class AB . . . . .	26
3.b.4. Class C . . . . .	27
3.b.5. Class D . . . . .	28
3.b.6. Class E . . . . .	28
3.c. Power Transistors . . . . .	29
3.d. Transmission Line . . . . .	31
<b>4. Power Amplifier Circuit Design</b>	<b>33</b>
4.a. Advanced Design System (ADS) . . . . .	33
4.b. MRF426 . . . . .	34
4.b.1. The project . . . . .	34
4.b.2. Simulation . . . . .	38
4.b.3. Fabrication . . . . .	40
<b>5. Experiments</b>	<b>42</b>
5.a. Experimental Protocol . . . . .	42
5.a.1. Vector Network Analyzer (VNA) . . . . .	42
5.b. Configuration 1: Just the PA . . . . .	42
5.c. Configuration 2: Using MTM with the PA . . . . .	46
5.c.1. Lightning up a LED . . . . .	46
5.c.2. Measuring Power . . . . .	49
<b>6. Conclusions</b>	<b>53</b>
6.a. Main Results . . . . .	53
6.b. Future Work . . . . .	53

## 1. Introduction

### 1.a. Historical Context

Despite the fact that it is a very popular and revolutionary research topic nowadays, the idea of WPT appeared in the 19th century, more specifically in 1899, when Nikola Tesla first theorized about transmitting electricity and signals without cables. In an attempt to overcome Hertz theories of radio waves, Tesla thought that if he injected electric current at the ground, creating a planar waveguide between ground and ionosphere, which are two conductive planes isolated from the atmosphere, he would be able to transfer data and power [10], no matter the distance. To appropriately test his ideas, he created a high voltage transformer in his Colorado Springs laboratory. After finding investors for his experiments, Tesla built the world's first power station, Wardencllyffe Tower (Figure 1), in Long Island, New York. Due to the great intensity of electric field, which significantly diminished the power transfer efficiency (PTE) and offers great danger to human beings, Tesla's invention could never be fully developed [11].

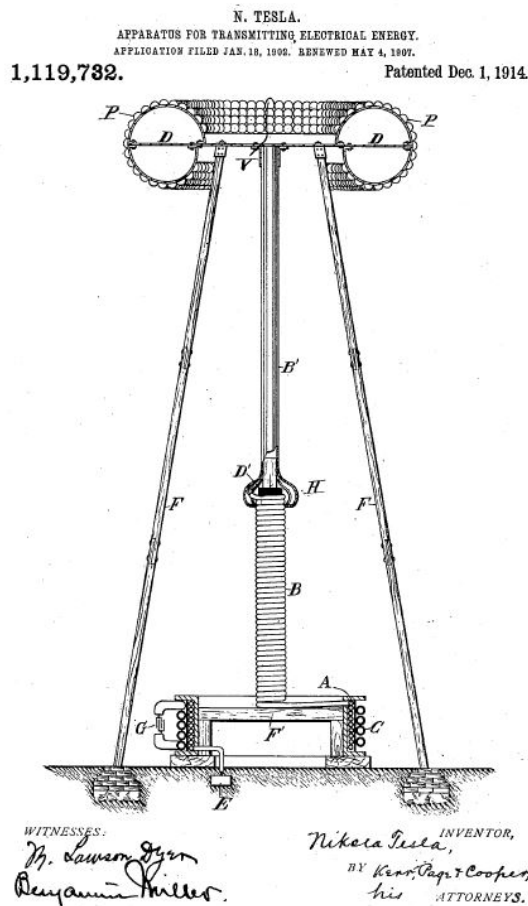


Figure 1: Wardencllyffe Tower

Available at: <http://www.teslascience.org/pages/questions.htm> [Accessed Date: 02/26/2018]

More than a century later, the interest in this topic was retrieved by the rising of wireless communications, electric and plug-in hybrid vehicles, wearables and so on. Everyday devices are facing a major engineering problem: batteries. Although it has been the unique tool used until now, it is expensive, heavy and not very efficient.

Three of the most famous WPT technologies are inductive coupling, magnetic resonant coupling and electromagnetic (EM) radiation. They are appropriately explained in Section 2.a. In this work, inductive coupling will be explored due to its cheap circuitry and easy implementation. Despite of these advantages, this technology becomes a challenge in terms of mobility and line of sight (LOS).

In 2010, the Wireless Power Consortium (WPC) approved the world's first wireless charging standard (Qi) for low-power inductive charging (< 5W) [11]. At this moment, the Qi specification is in its Version 1.2, being able to deliver 15 Watts of power [12].

In the industry, big corporations are investing in this area such as Apple and Samsung. According to Engadget, a technology enthusiastic blog, Apple acquired wireless charging company PowerbyProxi [13]. Thus, their new devices have wireless chargers and the Qi standard proposed by the WPC has been added to the iPhone 8, the iPhone 8 Plus and the iPhone X.

Even companies that are not related to this field are investing in this technology, like Disney. Last year they performed experiments with quasistatic cavity resonance (QSCR) to deliver wireless power within purpose-built structures, such as cabinets, rooms and warehouses (Figure 2) [14]. Although it is not the same kind of technology proposed in this work, it is possible to see how relevant and worldwide this topic is.

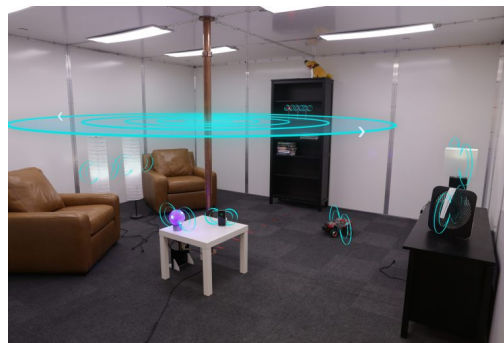


Figure 2: QSCR in the Disney Project.

Available at:

<https://www.disneyresearch.com/publication/quasistatic-cavity-resonance-for-ubiquitous-wireless-power-transfer/> [Accessed Date: 02/28/2018]

Simultaneously, in academia, this technology was very limited until 2007, when a team from the Department of Physics, Department of Electrical Engineering and Computer Science and Institute for Soldier Nanotechnologies, from MIT, was able to light a 60W light bulb from a power source seven feet away (approximately 2.13 meters). The distance achieved was up to 8 times the radius of the coils and the system could transfer energy with 40% of efficiency [15]. The experiment consisted of two self-resonant coils. One coil is coupled inductively to an oscillating circuit; the other is coupled inductively to a resistive load. Self-resonant coils use distributed inductance and distributed capacitance to achieve resonance. The experiment could match within 95% of what was expected theoretically. They refer to this concept as "WiTricity" (wireless electricity) and WiTricity Corporation was launched to take this technology forward from the MIT laboratories to commercial production [16].

Additionally, recent research from the Stanford Precourt Institute for Energy has achieved a whole new level. In June 2017, Professor Shanhui Fan and his graduate student Sid Assaworrorit developed a device that can wirelessly charge a moving object at close range. The technology could be used to charge electric cars on a highway (Figure 3), or medical implants and cellphones as people walk nearby [17].

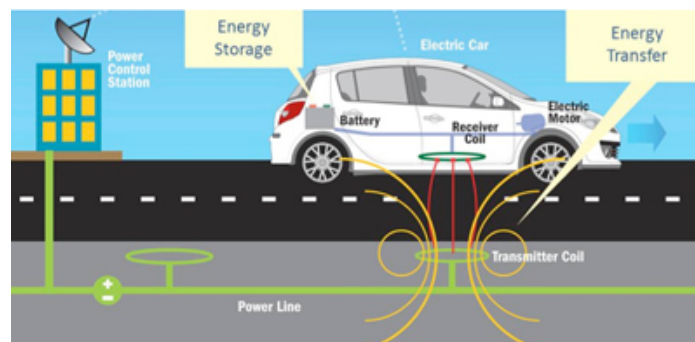


Figure 3: Electric car being charged while moving in a highway.

Available at: <https://sajadbangash.wordpress.com/2015/09/09/electric-cars-and-wireless-recharging-roads/> [Accessed Date: 02/28/2018]

Progresses in WPT with EM radiation have also been made. A team from the Department of Electrical Engineering from the University of Washington was able to successfully create a charging wireless system using near-infrared lasers [2]. Lasers provide a highly focused beam with high power density, so they are able to operate over long distances with minimal attenuation. Moreover, they can easily operate at powers exceeding a few watts. In contrast, human safety is still a major concern. Lasers in the visible wavelength at considerable power level can cause damage to the eye when exposed to a minimum amount of time (order of microseconds). One of the proposed solutions was to measure the reflected light from the receiver directly at the laser source. For this, they used retroreflectors (optimal element that reflects light back in the direction that it arrived) at the receiver. So, they created a low-power guard beam around the high power laser that is reflected by these retroreflectors and used photodiodes at the laser source to measure this reflected wave. For them to be able to have this reflection, as mentioned before, it is necessary to have LOS. By this, they were able to build a motion detection system that operates in the order of nanoseconds, so that when someone gets in the path of the high power laser beam, the system can quickly turn off (Figure 4).

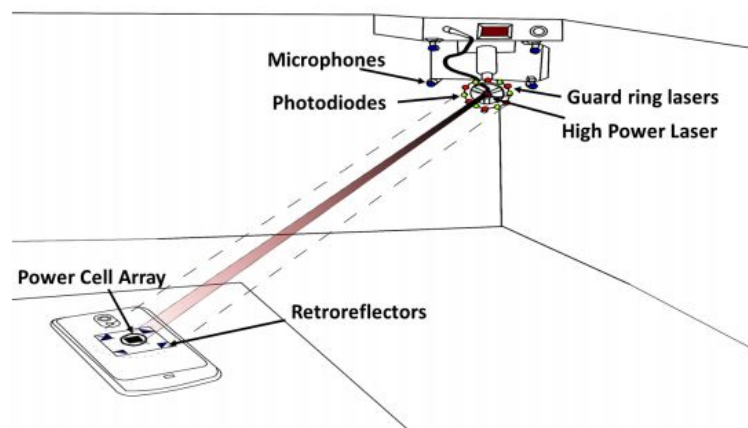


Figure 4: Laser based system for WPT. [2]

### 1.b. State of the Art

In previous works, an experimental setup of an IPT system assisted by MTM has been built at our laboratory [1]. In the present work, we will be focused on improving its power capability by adding a PA stage at the transmitter.

In terms of PA systems for IPT, the two main choices are Class D and Class E PAs [6]. In Section 3.b.5 and 3.b.6 operation principles and design considerations of both classes are then discussed.

The most important feature of non-linear PAs (Class D and Class E) as compared to linear PAs (Class A, Class AB) is the ideal unity efficiency ( $\eta_{ideal} = 100\%$ ). Since ideal switches have either zero turn-on voltage or zero turn-off current, these topologies consume a minimum amount of power, being useful then for high power efficiency designs [6].

Another challenge to IPT is variations in the impedance represented by the transmitter and receiver antenna of a system. When coupled, depending on the distance in between, the impedance of the antennas varies. For efficient IPT, a fully integrated power management using a method called Q-modulation was created [18]. Q-modulation is an adaptive scheme that offers load matching in a wide range of loading ( $R_L$ ) and coupling distance variations in inductive links to maintain high PTE. In a 1.45 W WPT setup, using a class E PA operating at 2 MHz, the system successfully increased the PTE.

In [19], it is also possible to see a solution concerning variations in load in an IPT system. Changes in load and range can shift the operation of the coil driver to a non-optimum switching state which results in higher switching losses and reduced output power levels. By controlling the duty cycle of a Class E inverter's switch and the value of its DC-feed inductance, the inverter can be tuned to operate at optimum switching conditions as the distance between coils changes.

Despite the fact that, in this project, there is a fixed coil impedance, which is very reactive, there were still challenges concerning how to match the PA with its load. This topic is deeply discussed in Section 3.d, Chapter 4 and Chapter 6.

Due to financial and technical limitations, and despite the obvious advantages of a switch-mode PA, a conventional linear PA (Class A) was implemented as proof of concept.

### 1.c. Objective

The objective of this work is to design and adapt a PA for a previously done project that introduced the use of MTMs in IPT [1]. By using the designed PA circuit and MTM slabs, the goal was to increase the distance between a transmitter and receiver coils and still be able to charge an electronic device. For the PA system, the power transistor MRF426 from MACOM was chosen [8]. Simulations and experiments with the MTM slabs are also planned in the scope of this project.

### 1.d. Chapters Description

Chapter 2 presents a brief review of the fundamentals of electromagnetism and explains the various WPT technologies. Also, an introduction to MTM theory is made and the models used in this work are presented.

Chapter 3 presents an introduction to bipolar junction transistor (BJT) theory and amplifiers topologies. Later on, a transmission line review is made, including the challenges of impedance matching with a very reactive load.

Chapters 4 presents the project developed in this work, including circuit design, simulation and fabrication.

Chapter 5 presents the obtained experimental results of the PA by itself and with MTM slabs and an light emitting diode (LED).

Chapters 6 presents the main conclusions and future works.

## 2. Theory

In this chapter, it is made a review of the different technologies available to deliver wireless power and the EM laws governing their transfer mechanism. Those technologies can be categorized as far field (EM radiation) or near field technologies (inductive coupling, magnetic resonant coupling). In the end of this chapter, there is a brief introduction to MTMs theory and a description of the ones used in this project.

### 2.a. Electromagnetic Theory

#### 2.a.1. Far Field vs. Near Field Regions

The space surrounding an antenna is subdivided in three areas: the reactive near field, the radiating near field (Fresnel Region) and the far field (Fraunhofer Region). According to [20], they can be distinguished by the following criteria shown below:

Table 1: Region Separation

Regions	Boundaries
Reactive near field	$r < 0.62\sqrt{\frac{D^3}{\lambda}}$
Radiating near field (Fresnel Region)	$0.62\sqrt{\frac{D^3}{\lambda}} \leq r < \frac{2D^2}{\lambda}$
Far field (Fraunhofer Region)	$\frac{2D^2}{\lambda} \leq r \leq \infty$

$D$  is the largest dimension of the antenna. It needs to be large compared to the wavelength ( $D > \lambda$ ).

Nonetheless, for antennas that are electromagnetically small (see Table 2), there are only two regions: the quasistatic field and the radiating field (Figure 5).

Table 2: Electromagnetically Small Antennas

Antenna Type	Relative Length
Small Dipole	$\lambda/50 < l \leq \lambda/10$
Small Loop	$a < \lambda/6\pi$

$l$  is the dipole length and  $a$  is the loop radius. In this case, the operating frequency is 13.56 MHz, so  $\lambda/6\pi$  would be 1.17 m, much more than the radius of the loop designed.

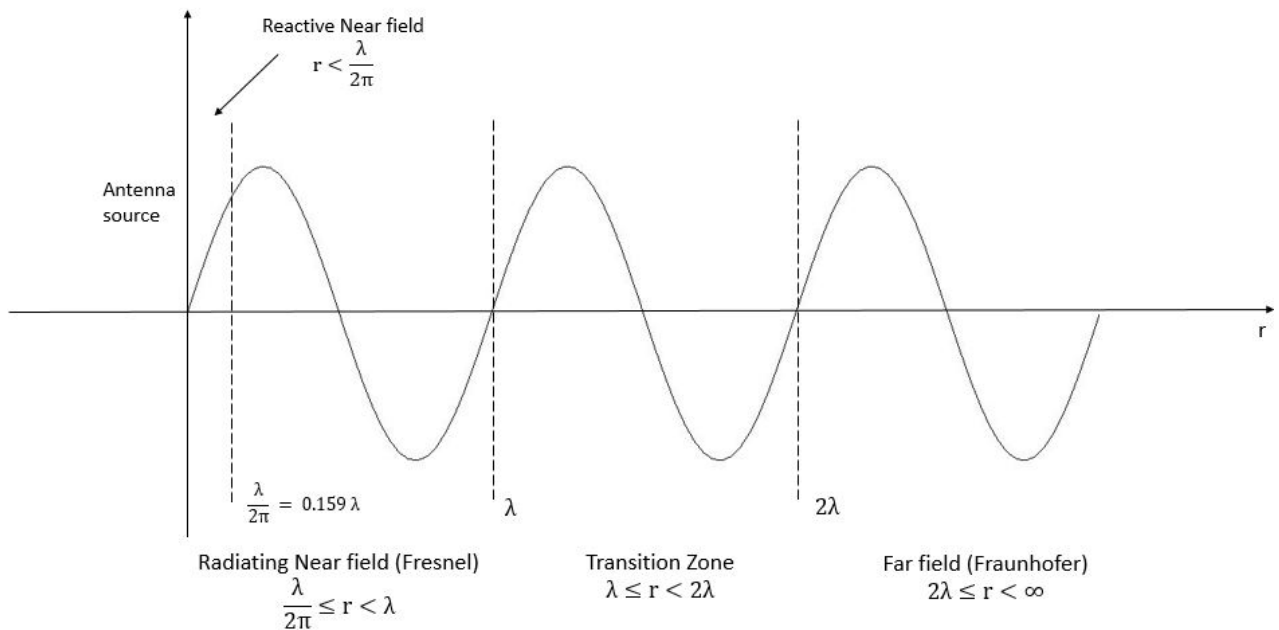


Figure 5: Space surrounding a small loop antenna

In these regions, the fields behave differently and the WPT technologies use these properties on their own advantage.

In the quasistatic region, one of the fields (the electric or the magnetic one) is dominant and the energy is kept stored as an electric or a magnetic potential. Differently from what happens in the radiating field, in this area, the waves do not detach from the antenna and almost no power is lost from the source in the absence of a proper receiver.

In the radiating field region, the energy propagates as EM radiation far from its source. Here, the electric and magnetic fields are perpendicular and their ratio is defined as the wave impedance  $\eta$  as shown in:

$$\vec{H} = \frac{\vec{E}}{\eta}. \quad (1)$$

In free space,  $\eta = 120\pi$  [21].

In Figure 6, in the near field region, if the electric field is predominant (e.g. dipole antenna), the wave impedance is high, which means that the electric field is much greater than the magnetic. Nonetheless, if the magnetic field is predominant (e.g. small loop), wave impedance is low, which means that the magnetic field is much greater than the electric. In the far field ( $r > \lambda/2\pi$ ), the wave impedance is defined by the medium.

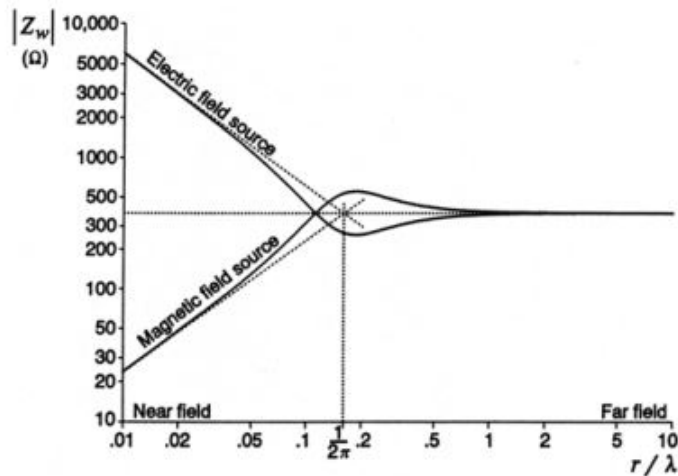


Figure 6: Wave Impedance as a function of Distance [1]

In this work the interest is to study the WPT technologies for near field region, such as inductive coupling and magnetic resonant coupling, and for the far field one, such as microwave power transmission (MPT) and laser charging. They will be explained in details in the following sections.

**2.a.2. Inductive Coupling**

Just as the physical principle that rules an electrical transformer, IPT also uses inductive coupling (Figure 7). This phenomenon can be exemplified by an alternating current in a primary coil that generates a varying magnetic field that induces a voltage across the terminals of the second coil, as indicated by Faraday's law in equation 2.

$$V_{fem} = \frac{-d\phi}{dt} = - \int \frac{\partial B}{\partial t} dS. \tag{2}$$

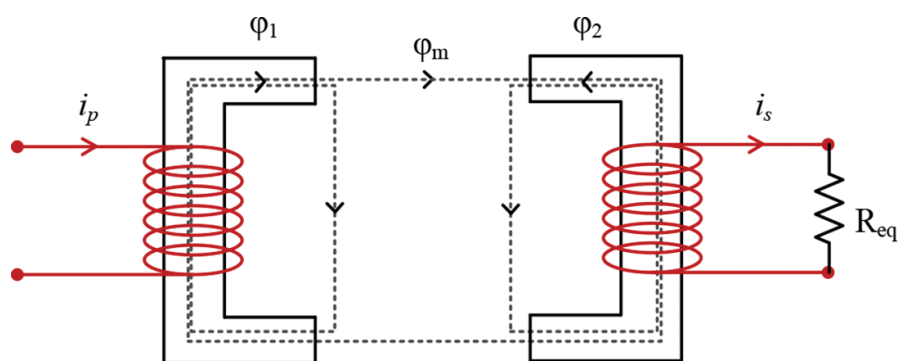


Figure 7: Electrical Transformer

Available at:  
<https://www.intechopen.com/books/wireless-power-transfer-fundamentals-and-technologies/fundamentals-of-inductively-coupled-wireless->  
 [Accessed Date: 03/22/2018]

According to [6], the voltage and current across the primary and secondary coils are related by the following matrix

$$\begin{bmatrix} V_1 \\ V_2 \end{bmatrix} = j\omega \begin{bmatrix} L_1 & M_{12} \\ M_{21} & L_2 \end{bmatrix} \begin{bmatrix} I_1 \\ I_2 \end{bmatrix}, \quad (3)$$

$V_1 \rightarrow$  Voltage Across the Primary Coil  
 $V_2 \rightarrow$  Voltage Across the Secondary Coil  
 $I_1 \rightarrow$  Current in the Primary Coil  
 $I_2 \rightarrow$  Current in the Secondary Coil  
 $L_1 \rightarrow$  Inductance in the Primary Coil  
 $L_2 \rightarrow$  Inductance in the Secondary Coil  
 $M_{12}$  &  $M_{21} \rightarrow$  Mutual Inductance between coils

$$\kappa = \frac{M_{12}}{\sqrt{L_1 \times L_2}} = \frac{M_{21}}{\sqrt{L_1 \times L_2}}, \quad (4)$$

being  $\kappa$  the coupling coefficient between the primary and secondary coils. For a perfect magnetic coupling,  $\kappa = 1$ . The power found in the primary and secondary coil can be defined by

$$P_1 = \frac{V_1^2 Z_2}{Z_1 Z_2 M_{12}}, \quad (5)$$

$$P_2 = \frac{V_1^2 (\omega M_{12})^2 R_2}{(Z_1 Z_2 + (\omega M_{12})^2)^2}. \quad (6)$$

The efficiency is given as

$$\eta = \frac{P_2}{P_1} = \frac{R_2 (\omega M_{12})^2}{Z_2 (Z_1 Z_2 + (\omega M_{12})^2)}, \quad (7)$$

where  $\omega$  is given by  $\omega = 2\pi f$  ( $f$  is the operating frequency).  $Z_1$  and  $Z_2$  are the impedances for the primary and secondary coil, respectively, where  $Z_1 = R_1 + jX_1$  and  $Z_2 = R_2 + jX_2$ . In this case,  $R_1$  and  $R_2$  are resistances and  $X_1$  and  $X_2$  are the reactances, from the primary and secondary coil, respectively.

Equation 7 shows that efficiency will grow with frequency. On the other hand, with higher frequencies, less distance can be achieved. Then, there is a balance between maximum distance and maximum PTE possible to be achieved. As a result, inductive coupling has better use in very short distances when the transmitter and the receiver are close in contact and have accurate alignment in the charging direction [11]. In Figure 8, some devices that use inductive coupling are shown:

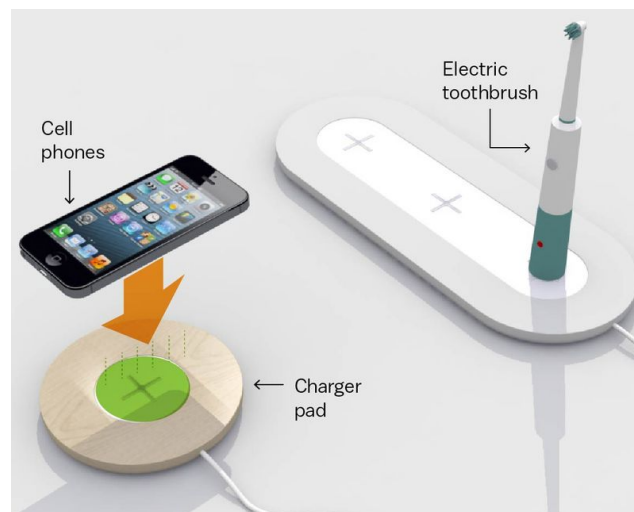


Figure 8: Devices that use inductive coupling

Available at: <https://www.vox.com/science-and-health/2017/1/17/13951274/wireless-charging-coming-soon> [Accessed Date: 03/26/2018]

### 2.a.3. Magnetic Resonant Coupling

The second type of WPT technology is magnetic resonant coupling. It is based on the well-known physical principle of resonance, where the energy of a system is oscillating between two components that are working in the same resonance frequency, so they are strongly coupled via non-radiative magnetic resonance induction [11]. In this case, these two components are capacitors and inductors, as any simple circuits example (Figure 9).

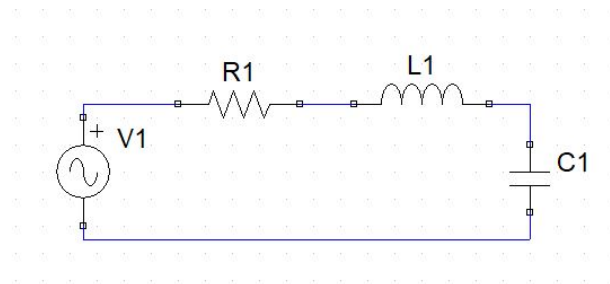


Figure 9: Resonant Circuit

It can be considered a special case of inductive coupling where the primary and secondary coils are tuned in resonance by adding compensation capacitors [11]. In this case, the coils (small loops) would be connected to capacitors and inductors and operating in the resonance frequency.

In magnetic resonant coupling, energy can be successfully transferred from a source coil to a receiving coil with little loss of energy and with greater distances compared to inductive coupling. Compared to EM radiation, magnetic resonant coupling has a higher PTE even under omni-direction, and not requiring LOS [11]. Due to the quality factor (Q-factor), it can operate efficiently even if the coupling coefficient ( $\kappa$ ) is too small ( $<0.2$ ) [1].

Yet, it still has technical challenges such as orientation and interference. If not co-axially aligned, the coils cannot achieve certain distances, since the coupling factor diminishes considerably. Moreover, when charging multiple devices, mutual coupling among various receiving coils may cause interference, which can only be solved by tuning these devices [11].

The energy injection rate for an isolated resonator can be defined as [6]

$$\omega_0 = \frac{1}{\sqrt{LC}}, \tag{8}$$

$$Q = \frac{\omega_0}{2\Gamma} = \sqrt{\frac{L}{C}} \frac{1}{R} = \frac{\omega_0 L}{R}, \tag{9}$$

where  $\omega_0$  is the resonance frequency,  $L$  is the inductance,  $C$  the capacitance,  $R$  the resistance,  $Q$  the quality factor and  $\Gamma$  the intrinsic rate of energy loss.

In Figure 10, there is an example of a coupled resonator system:

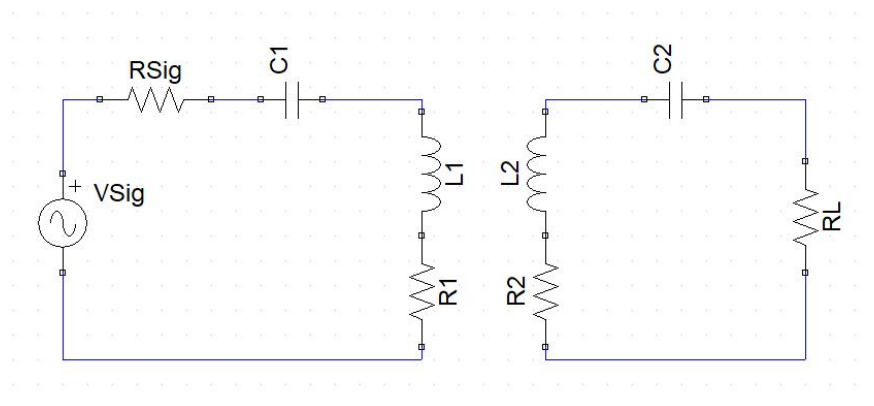


Figure 10: Coupled Resonator System

By circuit inspection, efficiency can be defined as [6]

$$\eta = \frac{P_L}{P_{Sig}} = \frac{1}{1 + \frac{n^2}{k^2} \frac{1}{Q_S^2} \frac{R_1}{R_L} + \frac{R_2}{R_L}}, \quad (10)$$

being

$$Q_S = \frac{\omega_0 L_2}{R_L + R_2}, \quad (11)$$

where  $\eta$  is the efficiency,  $P_L$  is the power on the load ( $R_L$ ),  $P_{sig}$  is the power on the source,  $n$  is the proportion (1:n) between coils,  $k$  the coupling coefficient and  $Q_S$  is the quality factors of the system given by Equation 11. The remaining parameters are indicated in Figure 10. The Q-factor in a parallel RLC circuit is the inverse of a Q-factor in a series RLC circuit. Derived from Equation 9 there is

$$Q_{series} = \frac{\omega_0}{2\Gamma} = \sqrt{\frac{L}{C}} \frac{1}{R} = \frac{\omega_0 L}{R}, \quad (12)$$

$$Q_{parallel} = \frac{2\Gamma}{\omega_0} = \sqrt{\frac{C}{L}} R = \frac{R}{\omega_0 L}. \quad (13)$$

In Figure 11, an application of magnetic resonant coupling is shown:



Figure 11: Qualcomm Halo Technology - Application of Magnetic Resonant Coupling

Available at: <http://www.sandiegouniontribune.com/business/sd-fi-wireless-car-charging-20170224-story.html> [Accessed Date: 06/12/2018]

## 2.a.4. EM Radiation

EM radiation consists on energy emission from a transmitting antenna of a power source to a receiving antenna via radiative EM waves. Differently from what happens in near field technologies (inductive coupling and magnetic resonant coupling), in this case, the waves "detach" from the antenna so, once they are transmitted, they never come back to its source, regardless of the presence of a receiving antenna [1]. Depending on its directivity, an antenna can be called omnidirectional or directional [11].

Omnidirectional antennas, for example, are not very good tools to WPT since the EM waves decay quickly over distance, resulting in a serious efficiency problem. Moreover, EM radiation interacts strongly with humans and electronic devices. So, caring high power would mean a serious health threat and would cause much more interference in daily devices. Then, it is only recommended for an ultra low-power sensor nodes, up to 10 mW, with very low sensing activities like temperature sensing [11].

Directional antennas for microwave or lasers can achieve high power transfer over a large distance when there is a clear LOS. In contrast, these devices require complicated tracking mechanisms to attend multiple devices, clear LOS and the inherent large scale of devices [11].

By the the wave equation of Helmholtz (Equation 14), it is possible to find the equations that define an uniform plane wave (UPW), [21]

$$\nabla^2 E = \mu\sigma \frac{\partial E}{\partial t} + \mu\epsilon \frac{\partial^2 E}{\partial t^2}. \quad (14)$$

The general solution for this equation is

$$E_S = (E_0^+ e^{-\gamma z} + E_0^- e^{+\gamma z}) \hat{x}, \quad (15)$$

where  $\gamma$  is the propagation constant,

$$\gamma = \sqrt{j\omega\mu(\sigma + j\omega\epsilon)} = \alpha + j\beta. \quad (16)$$

In Equation 16,  $\alpha$  is the attenuation,  $\beta$  is the phase constant,  $\omega = 2\pi f$  where  $f$  is the wave frequency,  $\mu$  is the magnetic permeability and  $\epsilon$  is the electric permittivity of the propagation medium. When the medium is free space, the electric permittivity is  $\epsilon_0 = 8.854 \times 10^{-12} F/m$  and the magnetic permeability is  $\mu_0 = 4\pi \times 10^{-7} H/m$ .

Its instantaneous general solution is

$$E(z, t) = E_0^+ e^{-\alpha z} \cos(\omega t - \beta z) \hat{x} + E_0^- e^{-\alpha z} \cos(\omega t + \beta z) \hat{x}. \quad (17)$$

Similarly, to the magnetic field there is

$$H_S = (H_0^+ e^{-\gamma z} + H_0^- e^{+\gamma z}) \hat{y} \quad (18)$$

and

$$H(z, t) = H_0^+ e^{-\alpha z} \cos(\omega t - \beta z) \hat{y} + H_0^- e^{-\alpha z} \cos(\omega t + \beta z) \hat{y}. \quad (19)$$

As mentioned previously in Equation 1, the relationship between the electric (E) and the magnetic field (H) is defined by the wave impedance,  $\eta$ . In this case, it is

$$\eta = \frac{E_0^+}{H_0^+} = \frac{E_0^-}{H_0^-}, \quad (20)$$

where  $\eta$  is,

$$\eta = \sqrt{\frac{j\omega\mu}{\sigma + j\omega\epsilon}}. \quad (21)$$

Additionally, the phase speed or propagation speed of a wave is defined by [21]

$$u_p = \frac{\omega}{\beta} = \frac{1}{\sqrt{\mu\epsilon}}. \quad (22)$$

The speed of a waveform is called group speed and is given by

$$u_g = \frac{\partial\omega}{\partial\beta}. \quad (23)$$

All these definitions are necessary to characterize an EM wave, in a transmission line, for example, given a specific medium and location.

## 2.a.5. Overview

In Table 3, a brief overview of the advantages, drawbacks and applications of each WPT technologies mentioned in this chapter is presented.

Table 3: WPT Advantages and Drawbacks

Technology	Advantage	Drawback	Application
Inductive Coupling	High power transfer in a distance of centimeters	Requires short charging distance and proper alignment	Electric toothbrushes, charging pads and medical implants
Magnetic Resonant Coupling	High efficiency with larger distances in all directions, doesn't require LOS	High power transfer only in a distance of a few meters	Charging mobile devices, electric vehicles
EM Radiation (Omnidirectional)	Tiny receiver size	Decays quickly over distance	Low power sensor nodes (e.g. Temperature monitoring)
EM Radiation (Directional)	High power transfer over long distances	Requires LOS, tracking mechanisms and inherently large scale devices	Charging mobile devices (UW Research)

This work explores the challenges of inductive coupling by the use of a PA system and MTM to increase the PTE.

## 2.b. Metamaterials

### 2.b.1. Theory

MTMs are artificial materials with periodic structures which its properties can be manipulated to obtain the response function of known materials or new response functions, impossible to be normally obtained. If desired, they can be designed to have negative electric permittivity ( $\epsilon$ ) and magnetic permeability ( $\mu$ ), depending on the application.

In this work, the interest was to use MTMs that are almost perfect lenses, with a refraction index ( $n$ ) smaller than zero [22]. They were designed to focus propagating and evanescent modes of an EM wave. Since the application is IPT, which is basically evanescent wave coupling, here, the interest is in the improvement of the operating distance. When focusing evanescent modes, the near field is amplified, enhancing the magnetic flux, and as a consequence, increasing the mutual coupling ( $\kappa$ ) between the coils [1]. In Table 4, it is presented a classification of MTMs and their properties.

Table 4: Types of MTMs

Type	Properties
Double Positive Media (DPS)	$\epsilon > 0$ and $\mu > 0$
Epsilon Negative Media (ENG)	$\epsilon < 0$ and $\mu > 0$
Double Negative Media (DNG)	$\epsilon < 0$ and $\mu < 0$
Mu Negative Media (MNG)	$\epsilon > 0$ and $\mu < 0$

To be able to build a perfect lens, the MTM has to have both negative  $\epsilon$  and negative  $\mu$ , or a double negative media MTM. This means that two artificial materials are combined, which can be very complex.

In double negative media, the refraction index is negative and thus, the group and phase velocities have opposite directions, instead of equal. Then, the energy flow goes in opposite direction to the movement of the wave fronts [3]. Moreover, this kind of property leads to a whole new phenomenon, where the evanescent EM waves of the near field are amplified, and the material works like a lens.

Inside materials with  $n < 0$ , a  $180^\circ$  phase shift is added to the propagating ray, having a discontinuity with the outside, which has no phase shift. When this discontinuity happens, a resonant phenomenon occurs at the interface in which the attenuating solution, caused by multiple reflections in the reactive near field, cancels out. As a result, only the growing solution stays, also caused by multiple reflections in the reactive near field (Figure 12). Respecting the conservation of energy law, the energy of the attenuating solution that was canceled out is transferred to the growing solution, enhancing its amplitude. As a conclusion, a negative magnetic reluctance is added, which diminishes the total magnetic reluctance between the transmitter and receiver coil. This negative magnetic reluctance increases the magnetic potential [1].

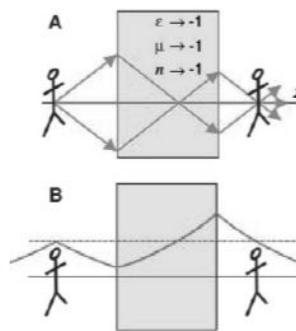


Figure 12: Focalizing the far field (A) and the near field (B) [3]

### 2.b.2. Models

After discussing the EM properties, the focus is on the desired unit-cell design for the MTM.

The first example of pattern model is the multiple split ring resonator (MSRR), that consists on N concentric split-rings with splits placed on the opposite sides of two consecutive rings (Figure 13). Split ring resonator (SRR), for example, is a MSRR with N=2.

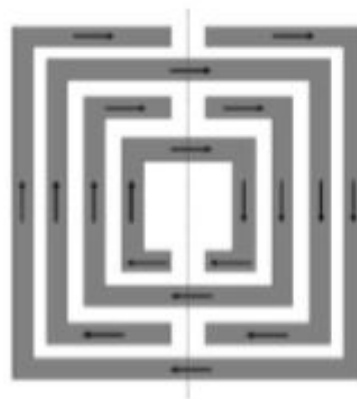


Figure 13: MSRR with N=4 [1]

According to [23], the total inductance and capacitance for this model can be defined as

$$L_{MSRR} = \frac{\mu_0}{2} \frac{l_{avg}}{4} 4.86 \left[ \ln \left( \frac{0.98}{\rho} \right) + 1.84 \rho \right], \quad (24)$$

$$C_{MSRR} = \frac{N-1}{2} [2l - (2N-1)(w+s)] C_0, \quad (25)$$

where  $l_{avg}$  is the average strip length calculated over all the  $N$  rings,  $\rho$  is the fill ratio,  $l$  is the side length of the outer ring,  $w$  is the strip width,  $s$  is the separation between two adjacent rings and  $C_0$  is the per-unit-length capacitance between two parallel strips. The parameters  $\rho$  and  $C_0$  can be defined as

$$\rho = \frac{(N-1)(w+s)}{l - (N-1)(w+s)}, \quad (26)$$

$$C_0 = \epsilon_0 \frac{K(\sqrt{1-k^2})}{K(k)}, \quad (27)$$

where  $K$  is the complete elliptic integral of the first kind and  $k$  is

$$k = \frac{\frac{s}{2}}{w + \frac{s}{2}}. \quad (28)$$

A certain  $N$  can be chosen to diminish the resonant frequency. However, this only works until a certain point, when, by increasing  $N$ , it will only finer the tune. [1].

A second example of pattern model is the spiral resonator (SR), which is the one that this project is most focused on. The SR model is a planar coil (Figure 14).

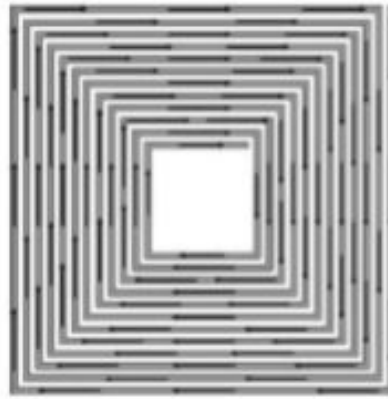


Figure 14: SR with N=12 [1]

According to [23], the total inductance and capacitance for this model can be defined as

$$C_{SR} = C_0 \frac{1}{4(w+s)} \frac{N^2}{N^2+1} \sum_{n=1}^{N-1} \left| l - \left( n + \frac{1}{2} \right) (w+s) \right|, \quad (29)$$

$$L_{SR} = \frac{\mu_0}{2\pi} l_{avg}^{SR} \left[ 1 + \ln \left( \frac{l_{avg}^{SR}}{2w} \right) \right], \quad (30)$$

$$l_{avg}^{SR} = \frac{4lN - [2N(1+N) - 3](s+w)}{N}, \quad (31)$$

where  $C_0$  is defined in Equation 27,  $w$  is the strip width,  $s$  is the separation between two adjacent rings,  $l_{avg}^{SR}$  is the single turn average length defined in Equation 31 and  $l$  is the side length of the outer ring.

As with the MSRR,  $N$  can be increased until a certain limit in order to decrease the resonant frequency [1].

Comparing these two models, the SR model presents a maximum linear dimension of the outer length smaller than the MSRR model. Additionally, for the same value of  $N$ , the SR model can achieve Q-factors 2 to 3 times greater than the MSRR model. This means that the SR model can achieve a more limited  $\Delta\omega$  and consequently, less coupling between the resonant system and free space, being able then to confine larger volumes of EM field [24]. Then, for this near field IPT application, the SR model is more suitable.

For this application, the goal is to transfer power with a distance in the order of meters. According to the wavelength ( $\lambda$ ), the frequency needs to be in the order of MHz. Nevertheless, according to what was discussed previously,  $N$  can be increased until a certain limit in order to decrease the resonant frequency. To work with

realistic sizes, the frequency needs to be in the order of GHz or greater. A solution for frequency adjustment is to add more capacitance or inductance to the circuit. As shown in the next section, for the first MTM design (13.56 MHz), a interdigital capacitor was added, and for the second one (33MHz), a CMS capacitor was added, in order to adjust the resonant frequency [1].

### 2.b.3. Design

For the experiments, it were used two types of MTM, one designed to work in 13.56 MHz and the other one in 33 MHz. It is important to emphasize that the design of these printed circuit boards (PCB) is not part of this work, but only one of the tools to perform experiments, obtain a higher gain and consequently, higher power transfer across two coils.

The first MTM is a SR cell since its quality factor is higher than of a SRR cell, considering the same dimensions. One of the objectives of this PCB is to have high inductance so that it can store enough magnetic field. It size was designed for realistic applications, within a few centimeters. To adjust the frequency, which was done experimentally, interdigital capacitors were used. Since the focus is on near field applications, the desire is to amplify magnetic field and for that, the MTM has to be a negative  $\mu$ . This design is also described in [24]. Below, a description of its characteristics is presented.

Substrate: FR-4

Characteristics of the substrate:

- $\rho = 10 \mu\Omega \text{ mm}$
- $\epsilon_r = 4.5$
- $\delta = 0.01$
- $w = 1.5 \text{ mm}$
- Dielectric Thickness = 1 mm
- Conductor Thickness = 35  $\mu\text{m}$

Prototype Parameters:

- $s = 1.0008 \text{ mm}$
- $w = 0.5994 \text{ mm}$
- $l = 7.6 \text{ cm}$
- Period of the lattice (center to center of the unit cells) = 8.1 cm

Total Conductor Dimensions:

- Length = 2850 mm
- Area = 0.02098  $\text{mm}^2$

Electric Resistance is given by the following expression:

$$R = \frac{\rho L}{A} = 1.358 \Omega. \quad (32)$$

SR Parameters:

As seen in Equation 29, 30 and 31, the following parameters were calculated by the expressions:

$$C_{SR} = C_0 \frac{1}{4(w+s)} \frac{N^2}{N^2+1} \sum_{n=1}^{N-1} \left| l - \left( n + \frac{1}{2} \right) (w+s) \right|,$$

$$L_{SR} = \frac{\mu_0}{2\pi} l_{avg}^{SR} \left[ 1 + \ln \left( \frac{l_{avg}^{SR}}{2w} \right) \right],$$

$$l_{avg}^{SR} = \frac{4lN - [2N(1+N) - 3](s+w)}{N}.$$

- $L_{SR} = 0.3311 \mu\text{H}$
- $C_{SR} = 2.1323 \text{ nF}$

Parameters in resonance using expressions 8 and 9:

$$\omega_0 = \frac{1}{\sqrt{L_{SR}C_{SR}}},$$
$$\omega_0 = 37.634 \text{ MHz},$$
$$Q = \sqrt{\frac{L_{SR}}{C_{SR}R}},$$
$$Q = 9.1760 \approx 9.$$

As mentioned previously, it was necessary to include in the back of the board interdigital capacitors so that the frequency is adjusted from 37.634 MHz to 13.56 MHz.

In Figure 15 and 16, it is shown the front and the back of this MTM:

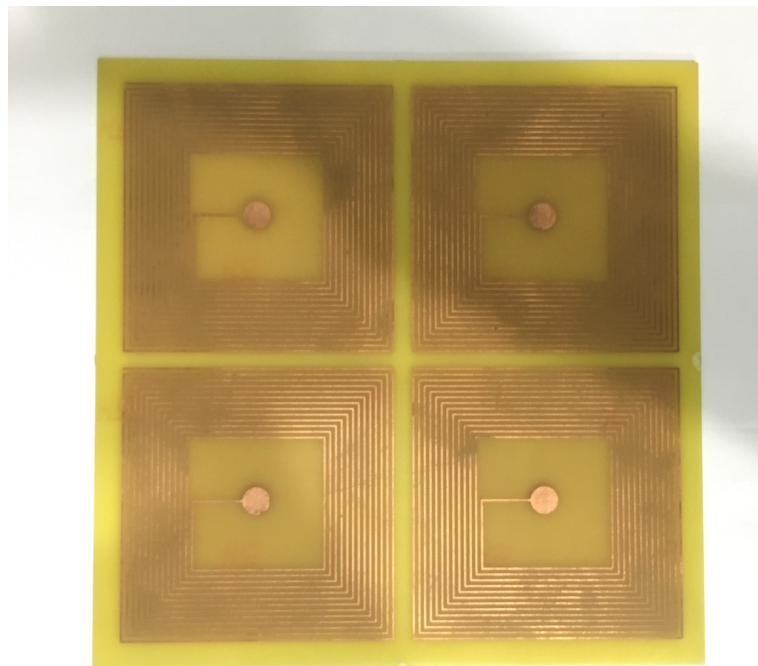


Figure 15: MTM for 13.56 MHz (front)

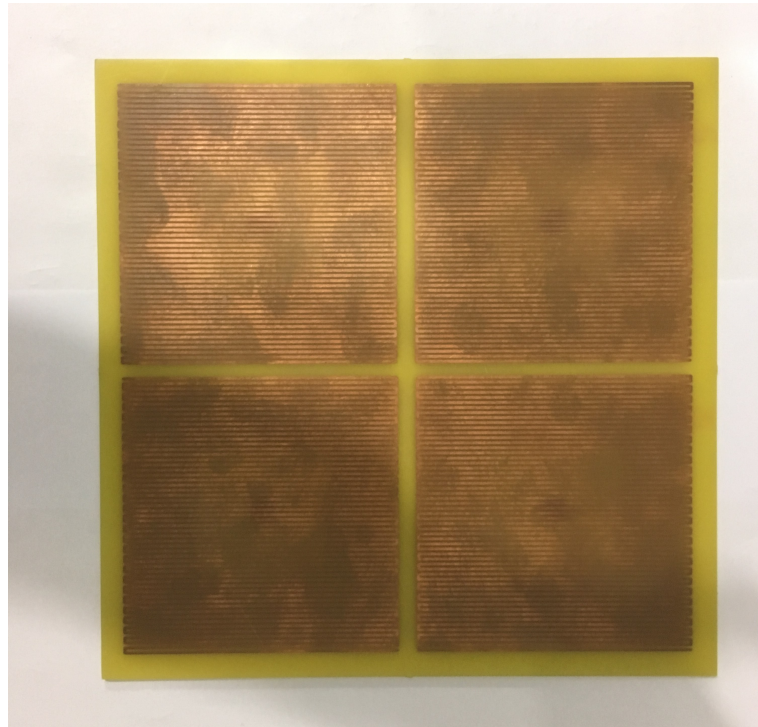


Figure 16: MTM for 13.56 MHz (back)

The second MTM (for 33 MHz) is also a SR cell and a double negative media, meaning both  $\mu$  and  $\epsilon$  are negative. Since its purpose is to amplify magnetic field, it only needed to be negative  $\mu$ . To regulate the resonance frequency, the MTM uses a lumped capacitor approach, so that it can stay in the range of tens of MHz. In the back of the PCB, there are CMS capacitors, connected with the inductor in the front of the slab via two holes (Figure 17). This design is also described in [1]. Below, its characteristics are described.

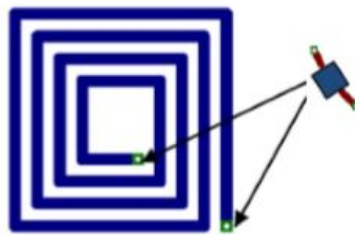


Figure 17: Lumped Capacitors connected in series with inductos via two holes. [1]

Substrate: FR-4

Characteristics of the substrate:

- $\rho = 10 \mu\Omega \text{ mm}$
- $\epsilon_r = 4.6$
- $\delta = 0.01$
- $w = 1.5 \text{ mm}$

Prototype Parameters:

- $d_{int} = 1 \text{ cm}$
- $d_{ext} = 2 \text{ cm}$
- $s = 1 \text{ mm}$
- $w = 1 \text{ mm}$

- CMS Capacitor = 100 pF
- Period of the lattice (center to center of the unit cells) = 2.3 cm  
Total Conductor Dimensions:
  - Length = 179 mm
  - Area =  $0.017 \text{ mm}^2$   
By expression 32  $R$  is:
    - $R = 0.2 \text{ } \Omega$ .  
By expression 30  $L_{SR}$  is:
      - $L_{SR} = 240 \text{ nH}$ .  
By expression 8 and 9  $f_0$  and  $Q$  are:
        - $f_0 = 33\text{MHz}$ ,
        - $Q = 180$ .  
Total Dimension:
          - Area =  $20 \text{ cm}^2$   
The software used for this design was Eagle 6.5.0.  
In Figure 18 and 19, the front and the back of this MTM are shown.

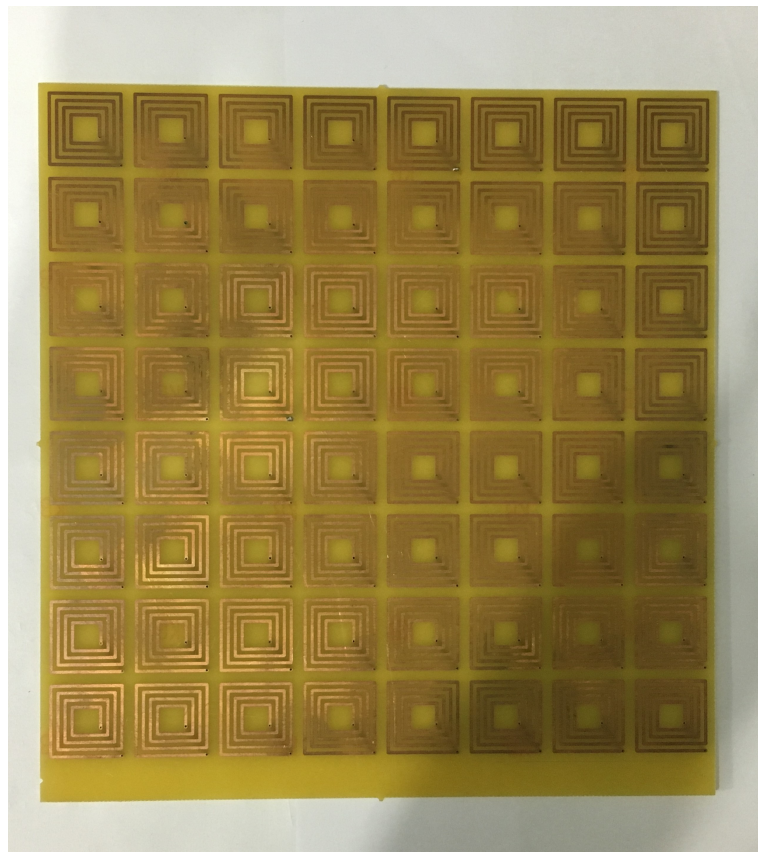
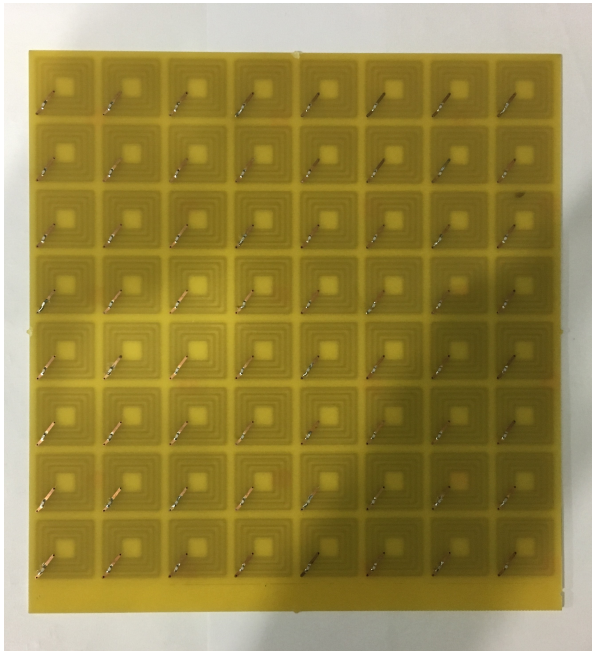
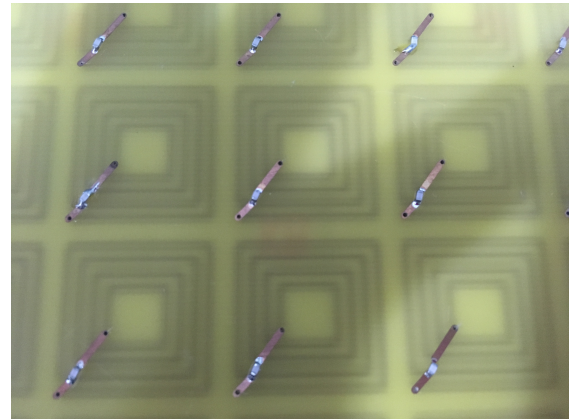


Figure 18: MTM for 13.6 MHz (front)



(a) MTM for 33 MHz (back)



(b) Capacitors in series with inductors

Figure 19: MTM for 33 MHz (back)

### 3. Theory of Power Amplifiers

In this chapter, an introduction to theory of amplifiers is made, including its classes, topologies with BJT, and polarization analysis. Here, the interest is in analyzing how to give power to a load efficiently, minimizing the dissipated power in the transistors.

To start this chapter, it is important to highlight some notations used. A signal can be described by

$$\begin{aligned} \text{DC Component} &\rightarrow V_A, \\ \text{AC Component} &\rightarrow v_a = V_a \text{sen}(\omega t) = V_a \text{sen}(2\pi ft), \\ \text{Signal} &\rightarrow v_A = V_A + v_a. \end{aligned}$$

Equivalently, the same can be done for the current.

#### 3.a. Bipolar Junction Transistor (BJT)

A BJT is a semiconductor device of three terminals: collector, base and emitter. It can be used for many different applications such as signals amplification and logic circuits. Through the adjustment in two of its terminals, collector and base, it is possible to control the emitter current. Differently from a metal oxide semiconductor field effect transistor (MOSFET), BJT controls current and not voltage. BJTs can be separated in two types: NPN and PNP, shown in Figure 20 [5].

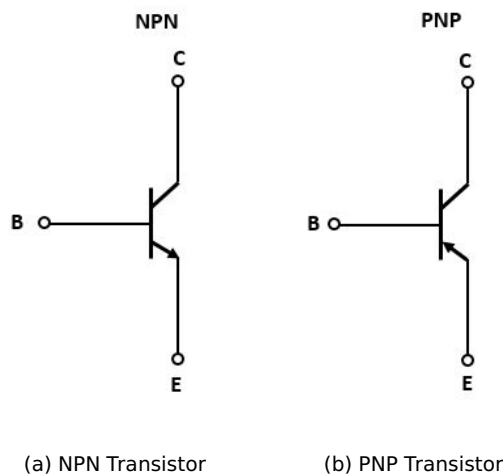


Figure 20: Two types of BJT

Moreover, the BJT can operate in three different regions: active, saturation and cutoff, according to Figure 21.

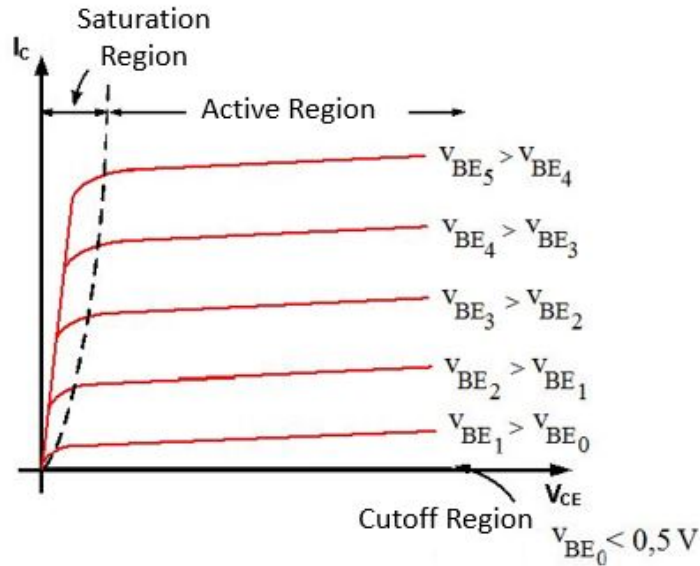


Figure 21: Operation Regions [4]

For a BJT NPN, these conditions are met [5]

Active Mode  $\rightarrow V_{BE} > 0.5 \text{ V}$  (usually  $V_{BE} = 0.7 \text{ V}$ ),  $V_{CB} > -0.5 \text{ V}$ ,  
 Saturation Mode  $\rightarrow V_{BE} > 0.5 \text{ V}$  (usually  $V_{BE} = 0.7 - 0.8 \text{ V}$ ),  $V_{CB} < -0.5 \text{ V}$ ,  
 Cutoff Mode  $\rightarrow V_{BE} < 0.5 \text{ V}$ .

In active region, which is the focus of this project, there are the following definitions,

$$i_B = \frac{I_S}{\beta} e^{v_{BE}/\eta V_t}, \quad (33)$$

$$i_C = \beta i_B, \quad (34)$$

$$i_E = i_C + i_B, \quad (35)$$

$$i_C = \alpha i_E, \quad (36)$$

$$\alpha = \frac{\beta}{\beta + 1}, \quad (37)$$

where  $i_B$  is the base current,  $I_S$  is the saturation current,  $\beta$  is the current gain,  $v_{BE}$  is the voltage between base and emitter,  $\eta$  is the emission coefficient,  $V_t$  is the thermal tension,  $i_C$  is the collector current and  $i_E$  is the emitter current [4].

When analyzing a BJT, there are usually two procedures that need to be done: polarization analysis (DC analysis) and analysis in a certain frequency band (AC analysis). In a DC analysis, all capacitors are considered open circuits and all inductors short circuits [4]. In Figure 22, there is an example of a common emitter topology:

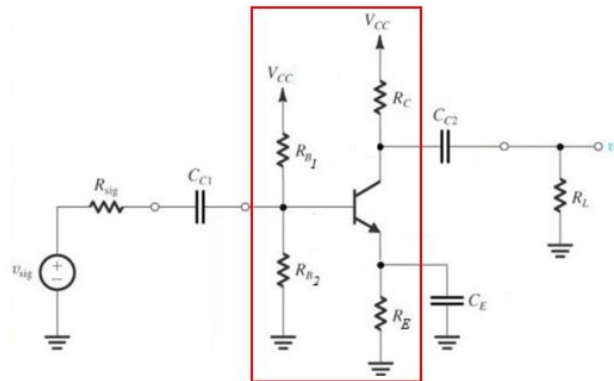
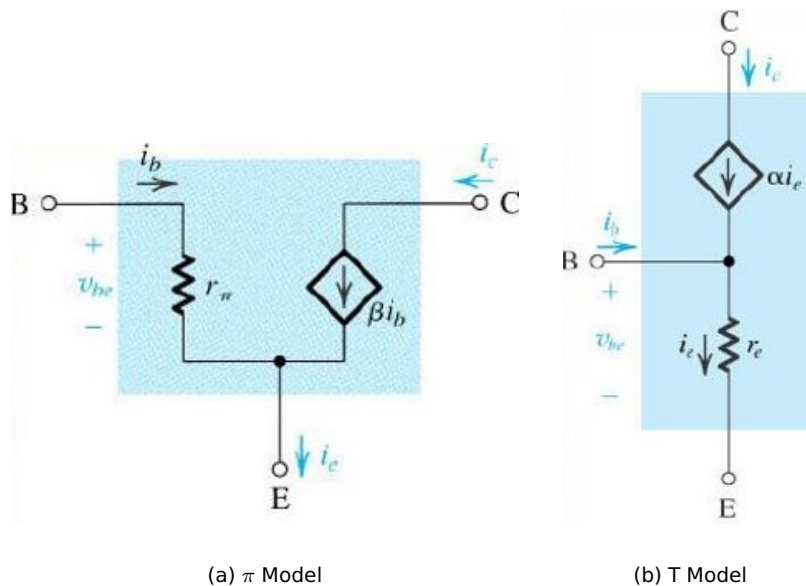


Figure 22: Common Emitter Topology [4]

In this case, in a DC analysis, only voltages and currents inside the red square are calculated.

Then, for the AC analysis, the capacitors and inductors are considered, in different ways, depending on the frequency band. Regardless of the frequency used, these two models,  $\pi$  Model and T Model, can be used for the analysis (Figure 23) [4].



(a)  $\pi$  Model

(b) T Model

Figure 23: Two types of BJT [4]

A few definitions are essential for these models [4]:

$$r_{\pi} = \frac{\beta}{g_m}, \tag{38}$$

$$r_e = \frac{\alpha}{g_m}, \tag{39}$$

$$g_m = \frac{I_C}{\eta V_t}. \tag{40}$$

It is important to remember that transconductance gain ( $g_m$ ) can only be defined after the DC analysis.

In Figure 24, it is presented a frequency response of a topology with BJT.

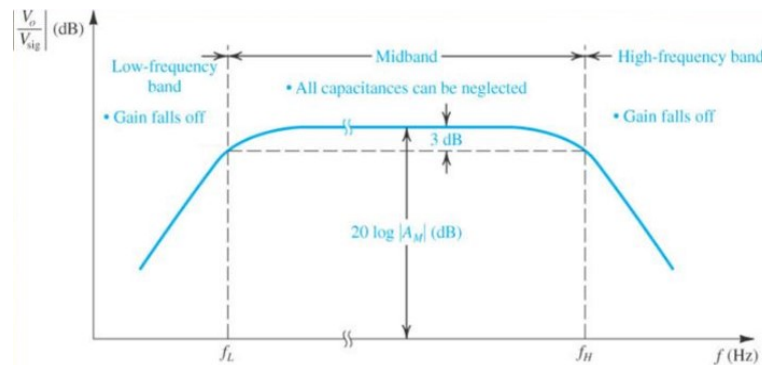


Figure 24: Frequency Response of a topology with BJT [4]

In a mid frequency band, external capacitances are considered short circuits and internal capacitances are considered open circuits [4].

In a low frequency band, external capacitances are considered with their exact values and internal capacitances as open circuits [4].

In a high frequency band, external capacitances are considered as open circuits and internal capacitances with their exact values [4].

In order to determine the transfer function of this kind of circuit, there are many different methods, including the Time Constant Method and Miller's Theorem. They are explained in details in [5].

### 3.b. Classes of Amplifiers

Amplifiers are classified depending on how their output stages are configured and operated. The main characteristics are linearity, signal gain, output power and efficiency. An amplifier class represents the type of output signal which varies within the amplifier circuit over one cycle of operation when excited by a sinusoidal input signal. This classification range from entirely linear operation (when a distortion of the signal is not desired) with very low efficiency, to entirely non-linear (when the signal format is not a priority) with much higher efficiency [25].

The first group explored is the most commonly used, with classes A, B, AB and C. They are conduction angle amplifiers where the length of their conduction state defines the output waveform [5].

The second group is the switch-mode amplifiers, with classes like D, E and many more. These amplifiers use digital circuits and pulse width modulation (PWM) to constantly switch between on and off, taking the transistor back and forth from saturation to the cutoff region [25].

#### 3.b.1. Class A

A class A amplifier is polarized with an  $I_C$  current greater than the signal amplitude of the current,  $\hat{I}_C$ . Therefore, the transistor conducts during the whole cycle of the input signal, having a conduction angle of  $360^\circ$  (Figure 25) [5].

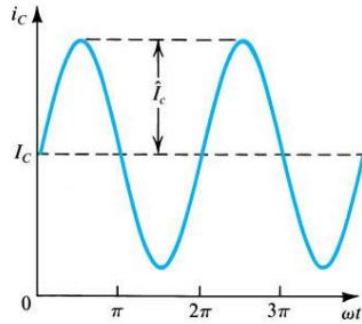


Figure 25: Output Waveform - Class A [4]

In Figure 26, an example of a class A amplifier circuit is shown:

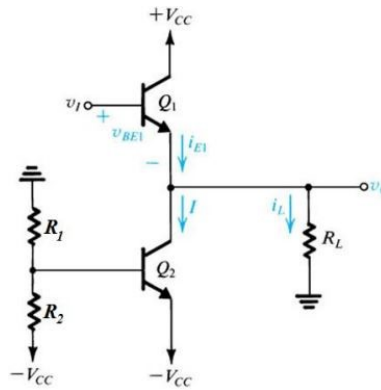


Figure 26: Circuit Example - Class A [4]

The graphic of the transfer function is given by:

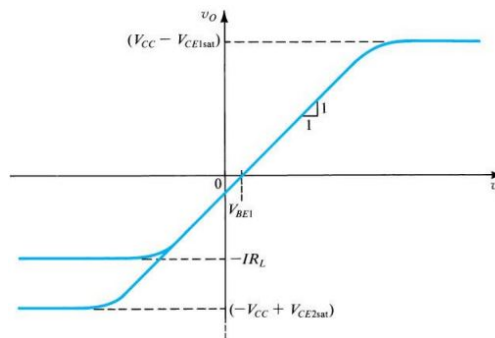


Figure 27: Transfer Function - Class A [4]

According to [5], the efficiency of the power conversion of an output stage is given by

$$\eta = \frac{P_L}{P_S}, \tag{41}$$

where  $P_L$  is load power and  $P_S$  is source power. For this class, supposing that the output is a senoidal waveform with peak value  $\hat{V}_o$ , the average load power will be

$$P_L = \frac{(\hat{V}_o/\sqrt{2})^2}{R_L} = \frac{1}{2} \frac{\hat{V}_o^2}{R_L}. \tag{42}$$

And, the power of the source is given by

$$P_S = 2V_{CC}I, \tag{43}$$

since the current in  $Q_1$  and  $Q_2$  is constant. Combining Equations 41, 42 and 43, the result is

$$\eta = \frac{1}{4} \frac{\hat{V}_o^2}{IR_L V_{CC}} \tag{44}$$

The maximum efficiency is given by  $\hat{V}_o^2 = V_{CC} = IR_L$ . So, the conclusion is that

$$\eta_{max} = \frac{1}{4} = 25\% \tag{45}$$

In realistic conditions, the efficiency usually is between 10% and 20%. Since it has a low efficiency, a class A amplifier is rarely used for applications that need more than 1W [5]. Nevertheless, due to its easy implementation, low cost and power capacity, a class A amplifier is more suitable for this work, even though it is not the most efficient.

### 3.b.2. Class B

A class B amplifier has its DC current  $I_C$  equal to zero. Consequently, the transistor only conducts on the semi positive cycle of the input signal, resulting in a  $180^\circ$  conduction angle (Figure 28) [5].

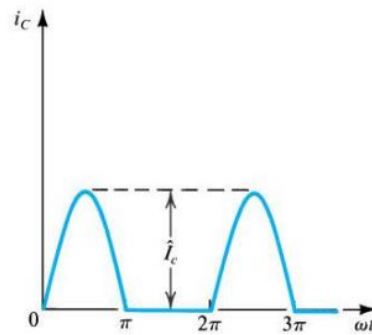


Figure 28: Output Waveform - Class B [4]

In Figure 29, an example of a class B amplifier circuit is shown:

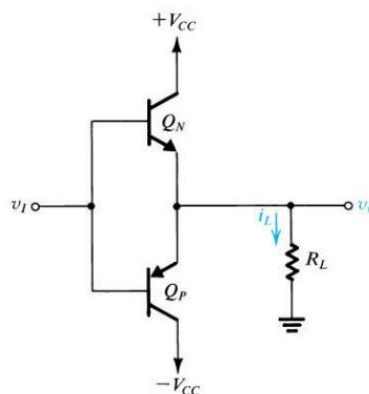


Figure 29: Circuit Example - Class B [4]

The graphic of the transfer function is given by:

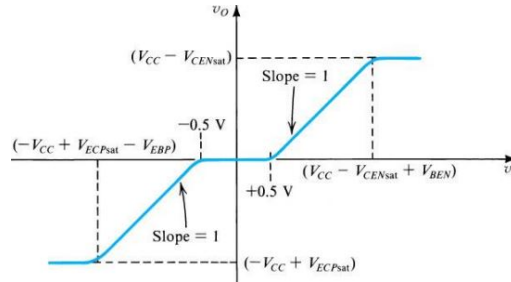


Figure 30: Transfer Function - Class B [4]

For this class, supposing that the output is a senoidal waveform with peak value  $\hat{V}_0$ , the average load power will be

$$P_L = \frac{(\hat{V}_o/\sqrt{2})^2}{R_L} = \frac{1}{2} \frac{\hat{V}_o^2}{R_L} \quad (46)$$

Also, the power of the source is given by

$$P_S = \frac{2}{\pi} \frac{\hat{V}_0}{R_L} V_{CC} \quad (47)$$

As a result, the efficiency is equal to

$$\eta = \frac{\left(\frac{1}{2} \frac{\hat{V}_0}{R_L}\right)}{\left(\frac{2}{\pi} \frac{\hat{V}_0}{R_L} V_{CC}\right)} = \frac{\pi}{4} \frac{\hat{V}_0}{V_{CC}} \quad (48)$$

The maximum efficiency happens when  $\hat{V}_0$  is maximum [5]. This maximum is limited by the saturation of  $Q_N$  and  $Q_P$  in  $V_{CC} - V_{CEsat} \approx V_{CC}$ . Therefore, when  $\hat{V}_0$  is maximum,  $\eta$  is

$$\eta_{max} = \frac{\pi}{4} = 78.5\% \quad (49)$$

It is noticeable that the efficiency of a class B amplifier is much higher than from a class A.

### 3.b.3. Class AB

In this class, the DC current,  $I_C$ , is bigger than zero but is much smaller than the signal amplitude of the current,  $\hat{I}_c$ . Then, the transistor conducts during a little more than the semi positive cycle of the input signal, resulting in a conduction angle between  $180^\circ$  and  $360^\circ$  (Figure 31) [5].

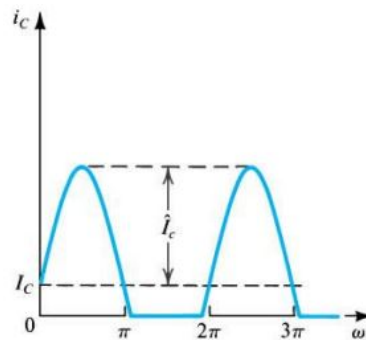


Figure 31: Output Waveform - Class AB [4]

In Figure 32, an example of a class AB amplifier circuit is shown:

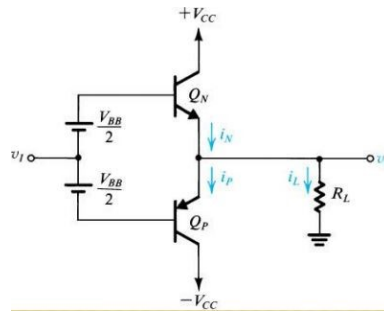


Figure 32: Circuit Example - Class AB [4]

The graphic of the transfer function is given by:

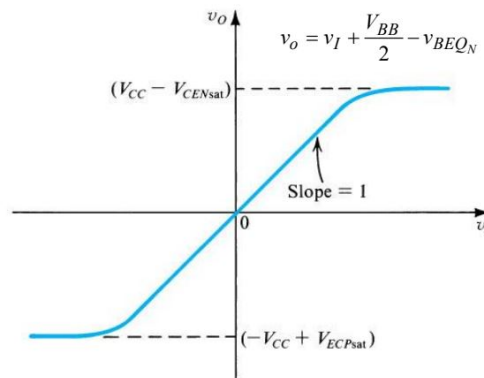


Figure 33: Transfer Function - Class AB [4]

Class AB is very similar to class B when it comes to efficiency. The only exception is that the polarization current  $I_Q$  elevates the power dissipation and reduces the amplifier efficiency. However, since  $I_Q$  is usually much smaller than the load current, the conclusion is that the losses in efficiency are not very significant [5]. Therefore, the efficiency in a class AB amplifier is

$$\eta \leq 78.5\% \tag{50}$$

### 3.b.4. Class C

Finishing the group of linear amplifiers there is class C. In this class, the conduction angle is less than  $180^\circ$ . The result is a current waveform pulsing periodically. To obtain a senoidal output waveform, the current goes through a kind of low pass filter, a LC circuit in parallel, tuned to work in the input frequency. In Figure 34, the output waveform of a class C amplifier is shown [5].

In the linear amplifiers group, the class C amplifier is the one with the highest efficiency due to the fact that the active device is biased beyond cutoff with a negative  $V_{BB}$  supply. This kind is most commonly used in radio frequency (RF) applications where a resonant circuit must be placed at the output in order to keep the sine wave going during the nonconducting portion of the input cycle [26].

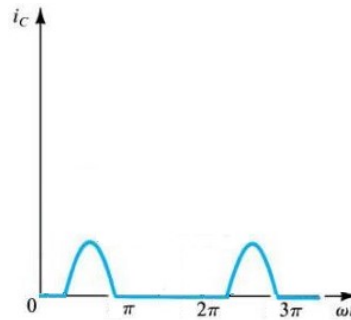


Figure 34: Transfer Function - Class C [5]

### 3.b.5. Class D

One of the main choices of PA for WPT are class D and E amplifiers. They are used to amplify the power of the digitally modulated input signal to be sent out by a transmitter and work similarly to a DC-AC converter. The key feature of non-linear amplifiers, as compared to linear amplifiers, is the ideal unity efficiency [6].

In Figure 35, an example of a class D amplifier circuit is shown:

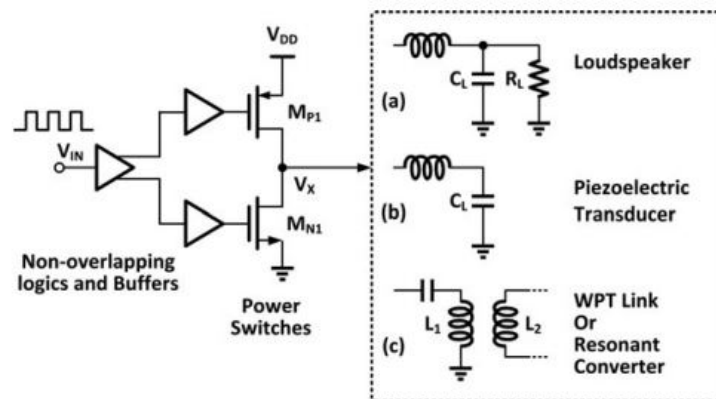


Figure 35: Circuit Example - Class D [6]

A complementary metal oxide semiconductor (CMOS) implementation of a class D amplifier consists of non-overlapping logic, gate-drive buffer and two power switches. Its operation is similar to that of a buck DC-DC converter. On the other hand, the difference is that the class D amplifier controls the output voltage pulses according to the varying input signal, while the buck converter takes a constant input signal and delivers a constant output voltage. When it comes to amplifying the signal of a WPT link, the load along with the resonant tank on the secondary coil can be modeled as an equivalent load impedance  $Z_{eq}$  reflected back to the primary coil that will affect the resonance frequency  $f_R$  of the primary LC tank. It is difficult to match the switching frequency  $f_S$  of the amplifier exactly with the resonance frequency in real implementations [6].

### 3.b.6. Class E

The second non-linear amplifier analyzed is the class E amplifier. For WPT, it consists of a single switch MN, an RF choke LC, a shunt capacitor CP, and an LC series resonant tank that contains CS and the coupling coils L1 and L2 (Figure 36). The inductance value of LC is set to be sufficiently high, resulting in a signal amplitude of the AC current smaller than the DC current, just as in class A amplifiers. The load network CP, CS and L1 is a combined series-parallel resonant circuit, which is also known as a multi-frequency network. The class E amplifier's operation results in high-power conversion efficiency at high frequencies. Its main applications are in communication transceivers, electronic ballasts for fluorescent lighting, heat induction, electrosurgical generator and WPT systems [6].

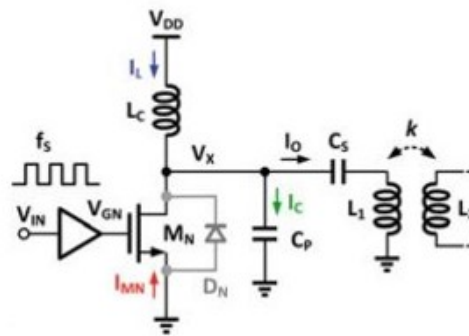


Figure 36: Circuit Example - Class E [6]

Although these non-linear amplifiers have an ideal efficiency of 100%, in practice, class E amplifiers can be more efficient than class D. In contrast, the normalized output power capability of the class D amplifiers is higher than that of the class E, which may limit the application of the class E amplifiers in high-power applications [6].

### 3.c. Power Transistors

BJT that are capable of dealing with a few ampères of current and power greater than 1W are called power BJT [4]. An RF amplifier using BJT usually works between 2 and 10 GHz. Normally, outside this range, they are considered as a low frequency electronic device [7]. Considering that, in this application, the operating frequency is 13.56 MHz, with a 30 MHz transistor, it is possible to consider it as a low frequency operation. Even so, due to the fact that the project includes microstrips and a very reactive load, transmission line concepts and impedance mismatch still need to be considered.

Power BJT dissipate great amount of power in its semiconductor junction. This dissipated power is converted to heat and increases the junction’s temperature. Then, this value cannot exceed a maximum point, where it can cause irretrievable damage. The dissipated power temperature ( $T_J$ ) can be defined as [4]

$$T_J = T_A + \theta_{JA} P_D, \tag{51}$$

where  $T_A$  is the room temperature,  $\theta_{JA}$  is the thermal resistance between the junction and the environment ( $^{\circ}C/W$ ) and  $P_D$  is the dissipated power. In Figure 37, a graphic of  $P_{D\text{MAX}}$  vs.  $T_{J\text{MAX}}$  is shown, where  $P_{D\text{MAX}}$  is the maximum dissipated power and  $T_{J\text{MAX}}$  is the maximum temperature caused by dissipated power.

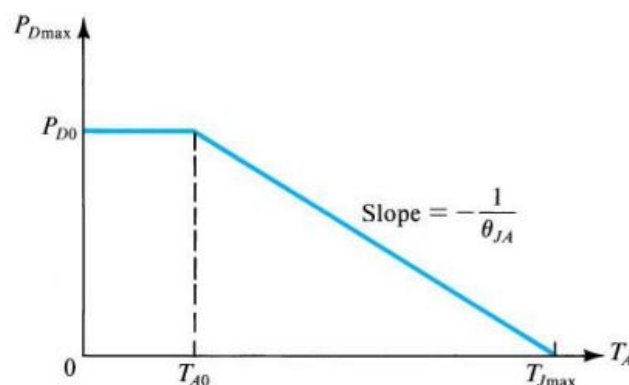


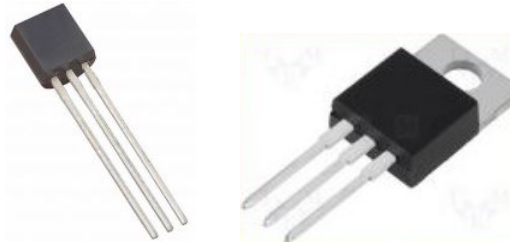
Figure 37: Circuit Example - Class E [4]

Additionally, the thermal resistance is given by

$$\theta_{JA} = \theta_{JC} + \theta_{CA}, \tag{52}$$

where  $\theta_{JA}$  is the thermal resistance between the junction and the environment,  $\theta_{JC}$  is the thermal resistance between the junction and the encapsulation and  $\theta_{CA}$  thermal resistance between the encapsulation and the

environment [4]. Normally,  $T_{JMAX}$ ,  $\theta_{JA}$  and  $\theta_{JC}$  are defined in the datasheet. In Figure 38 and 39, there are different types of encapsulation.



(a) Low Power

(b) Medium Power

Figure 38: Low and Medium Power BJT [4]



Figure 39: High Power [4]

To be able to adjust  $\theta_{CA}$ , the designer can add a heat sink to the encapsulation. In this situation,  $\theta_{CA}$  is defined as

$$\theta_{CA} = \theta_{CS} + \theta_{SA}, \quad (53)$$

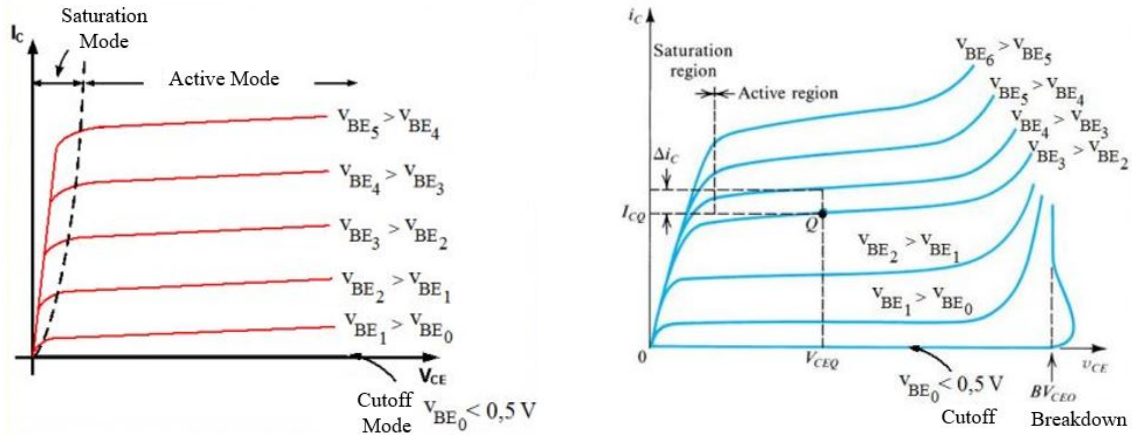
where  $\theta_{CA}$  is the thermal resistance between the junction and the environment,  $\theta_{CS}$  is the thermal resistance between the encapsulation and the heat sink and  $\theta_{SA}$  is the thermal resistance between the heat sink and the environment, which is highly dependent on the heat sink chosen [4].

Therefore, a BJT attached to a heat sink has a thermal resistance of

$$\theta_{JAdiss} = \theta_{JC} + \theta_{CS} + \theta_{SA}. \quad (54)$$

Due to its dimensions and elevated current values, a power BJT has different characteristics compared to a signal BJT. It is mandatory that the BJT has a  $\eta = 2$  and a low common-emitter current gain,  $\beta$  (usually between 30 and 80). Moreover, the internal capacitances,  $C_{\pi}$  and  $C_{\mu}$  are low, resulting in a frequency response deterioration in high frequencies. To conclude, the breakdown voltage,  $BV_{CEO}$  is higher, usually between 50V and 100V and being able to get to 500V [4].

In Figure 40, a comparison between graphics for a common-emitter topology is shown.



(a)  $I_C$  vs.  $V_{CE}$  [4]

(b)  $i_c$  vs.  $v_{CE}$  [4]

Figure 40: Comparison between DC component and the complete signal

### 3.d. Transmission Line

Even though this work is considered as a low frequency operation, evaluations of the challenges of a mismatched load still need to be done. In order to analyze the developed microstrip, a comprehension of the EM laws that regard a transmission line is necessary.

Just as in EM radiation seen in section 2.a.4, the voltage and current across a microstrip are also propagating waves. They can be defined by [7]

$$V(z) = V^+ e^{-\gamma z} + V^- e^{+\gamma z}, \tag{55}$$

$$I(z) = \frac{\gamma}{R + j\omega L} (V^+ e^{-\gamma z} + V^- e^{+\gamma z}), \tag{56}$$

where the characteristic impedance is given by,

$$Z_c = \sqrt{\frac{R + j\omega L}{G + j\omega C}} = \frac{\gamma}{R + j\omega L} = \frac{V(z)}{I(z)} = \frac{V^+}{I^+} = \frac{V^-}{I^-}. \tag{57}$$

In Equation 55 and 56,  $\gamma$  is defined by Equation 16. As seen in Figure 41,  $V^+$  and  $I^+$  are the voltage and current waves propagating towards the load. On the other hand,  $V^-$  and  $I^-$  are the voltage and current waves propagating towards the generator.

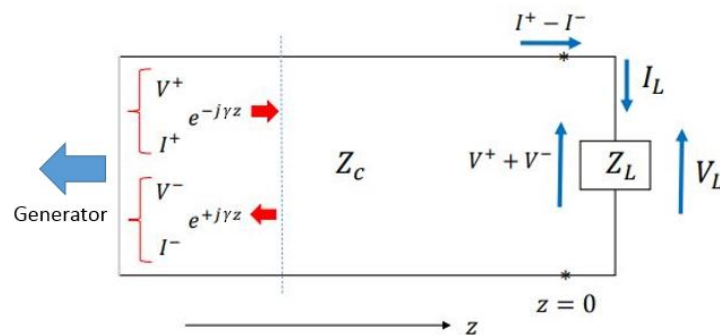


Figure 41: Transmission Line [7]

When the load,  $Z_L$ , is not matched with the transmission line, meaning,  $Z_c = Z_L$ , necessarily it is going to exist a  $V^-$  and  $I^-$ , which might affect the generator. In order to measure this back wave, the reflection coefficient needs to be defined, given by [7]

$$\Gamma_L = \frac{Z_L - Z_c}{Z_L + Z_c} = \frac{V^-}{V^+}. \quad (58)$$

In any point of the transmission line,  $\Gamma$  is given by [7]

$$\Gamma(-l) = \frac{V^- e^{-j\beta l}}{V^+ e^{j\beta l}} = \frac{V^-}{V^+} e^{-2j\beta l} = \Gamma_L e^{-2j\beta l}. \quad (59)$$

Additionally, the power delivered to the source when the load is mismatched is given by [7]

$$P_{tr} = \frac{1}{2} Y_c |V^+|^2 (1 - |\Gamma_L|^2), \quad (60)$$

$$P_{tr} = P_{inc} - P_{ref}, \quad (61)$$

$$P_{ref} = |\Gamma_L|^2 P_{inc}, \quad (62)$$

$$P_{tr} = P_{inc}(1 - |\Gamma_L|^2). \quad (63)$$

Then, the concept of return loss ( $L_R$ ) can be also introduced as [7]

$$L_R = 20 \log(\Gamma_L). \quad (64)$$

A very important parameter to establish is the voltage stationary wave rate (VSWR). A waveform is formed from the combination between the incident and reflected waveform. The measure between the maximum and minimum amplitude of this wave is called VSWR, which is defined as [7]

$$VSWR = \frac{|V_{max}|}{|V_{min}|} = \frac{1 + \Gamma_L}{1 - \Gamma_L}. \quad (65)$$

When the load is matched,

$$\Gamma_L = 0,$$

$$VSWR = 1,$$

$$L_R = \infty.$$

If the load is mismatched,

$$0 < \Gamma_L < 1,$$

$$1 < VSWR < \infty.$$

With the chosen BJT, MRF426, the maximum allowed VSWR is 30 [8]. Applying in Equation 65, a reflection coefficient of  $\Gamma_L = 0.9354$  is obtained, meaning that most of the incident waveform in this circuit can be reflected back to the BJT without damaging it. Using Equation 64, the return loss is  $L_R = -0.5793$ . Although impedance matching was considered in this work, in order to avoid reflected waves, the chosen component proved to be extremely resistant to this kind of problem.

#### 4. Power Amplifier Circuit Design

As explained in Section 1.c , the objective of this work is to create an amplifying system for a previous experiment [1].

In this previous work, the author attempted to use MTMs in IPT, in order to increase the distance between the transmitter and receiver antennas. In Figure 42, there is a block diagram that explains the old experiment.

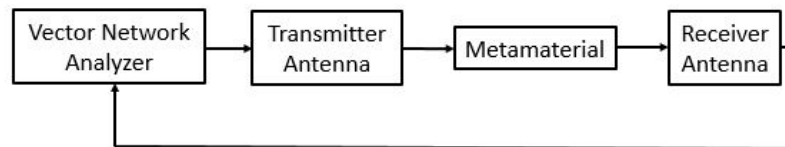


Figure 42: Old Experiment

In this work, the desire is to set even greater distances between the transmitter and receiver antennas. By a combination between the PA and the MTMs presented in Section 2.b.3, the goal is to increase this distance and try lighting up a LED or charging a smartphone. In Figure 43, there is a block diagram that explains the new experiment.

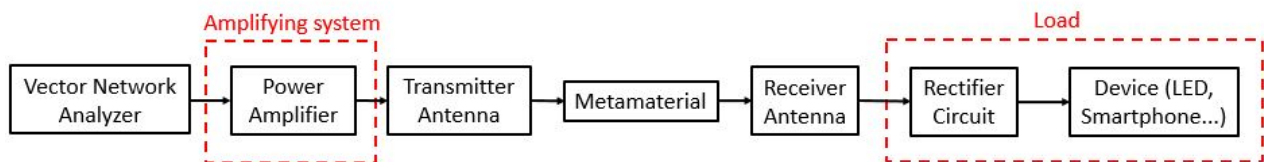


Figure 43: Amplifying System

##### 4.a. Advanced Design System (ADS)

ADS is an electronic design automation software for RF, microwave, high speed digital, and power electronics applications. It has been created by Keysight EEsof EDA, a division of Keysight Technologies (formerly Agilent's Electronic Measurement). By offering technologies such as 3D EM simulators and X parameters, the software has been used by leading companies in the wireless communication & networking, aerospace & defense, automotive, and energy industries [27].

Keysight ADS is a useful tool in every step of the design process, including schematic tools, layout, frequency and time domain circuit simulations and EM simulations.

For WiMAX™, LTE, multi-gigabit per second data links, radar, satellite, and switched-mode power supply designs, ADS provides standards-based design and verification with Wireless and other Application-specific Libraries and EM simulations in an integrated platform [27].

Integrated with ADS, there is Momentum:3D planar EM simulation software for electronics and antenna analysis based on method of moments. It accepts multiple designs and by using method of moments, it can precisely simulate complex EM effects including coupling and parasitic [1].

In this project, it was used ADS 2016.

## 4.b. MRF426

### 4.b.1. The project

The chosen BJT was the MRF 426, an RF Line NPN Silicon Power Transistor from MACOM. In 30MHz with 28V, it is expected to deliver 25 W, have a minimum gain of 22 dB and efficiency of 35%. Since the proposed work is designed for 13.6 MHz, the expectations are a little different. Moreover, for load mismatch at all phase angles, it promises a VSWR of 30:1. This BJT can only be used for A or AB amplifier topologies [8].

As an initial model for the PA circuit, the decision was to follow the datasheet proposed schematic as shown in Figure 44, and make adjustments. It is important to highlight the use of this tuning capacitors ( $C_1$ ,  $C_2$ ,  $C_3$  and  $C_4$ ). After experimental observation, it was noticeable that  $C_1$  and  $C_2$  are used to filter high frequencies, and  $C_3$  and  $C_4$  are used to amplify high frequencies. Moreover, when filtering high frequencies, it was observed a little amplification of the signal in low frequencies. Since the focus is in the low part of the frequency band, the capacitors were tuned in order to operate at its optimum point in 13.6 MHz.

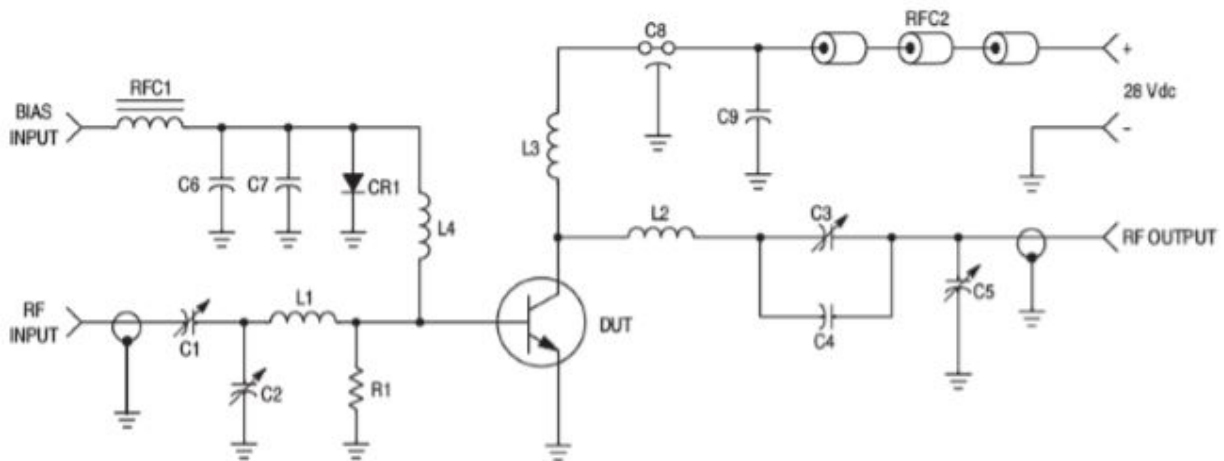


Figure 44: First Schematic [8]

In Table 5, a more detailed description of each and every component is presented. The three distributors used in this work were Digikey, RF Parts and Dexter Magnetic Technologies.

Table 5: Initial Model's Components

Components	Specifications	Manufacturer
C1, C2	469 Trimmer, Compression Mica Capacitor, 215-790 pF	ARCO Electronics
C3, C4	S464 Trimmer, Variable Compression Mica Capacitor, 45-280 pF	ARCO Electronics
C5	Mica Capacitor, 120 pF	Cornell Dubilier Electronics
C6, C7	Ceramic Capacitor, 100 $\mu$ F, 25V	United Chemi-Con
C8	Ceramic Capacitor, 680 pF, 500V	KEMET
C9	Tantalum Capacitor, 1 $\mu$ F, 35V	AVX Corporation
L1	3 turns, AWG 10, 8.4mm, 60 nH	N/A
L2	6 turns, AWG 10, 15.9mm, 0.68 $\mu$ H	N/A
L3	7 turns, AWG 10, 14.mm, 0.76 $\mu$ H	N/A
L4	Fixed Inductor, 10 $\mu$ H	Würth Electronics Inc.
CR1	Diode, 1N4997	Motorola
R1	Resistor, 10 $\Omega$ 1/2W	Vishay Dale
RFC1	Wound Ferrite Bead	Ferroxcube
RFC2	Ferrite Sleeve	Ferroxcube

For the inductors L1, L2 and L3, the datasheet suggested actual coils with different wires and loop diameters, instead of lumped components. Since these specific wires were not available, the decision was to use AWG 10 and calculate new loop diameters that would give the same inductance. To achieve this equivalency, the following expression was used [28]

$$L_{coil} = N^2 \mu_0 \mu_r \left( \frac{D}{2} \right) \left[ \ln \left( \frac{8D}{d} \right) - 2 \right], \quad (66)$$

where  $L_{coil}$  is the coil inductance,  $N$  is the number of turns,  $D$  is the loop diameter and  $d$  is the wire diameter. Then, the new coils have the following characteristics:

Table 6: Inductance Equivalency

Component	Inductance	Datasheet	Equivalent
L1	60.05 nH	3 turns, 16 AWG, 6.35 mm	3 turns, 10 AWG, 8.4 mm
L2	0.679 $\mu$ H	6 turns, 16 AWG, 12.7 mm	6 turns, 10 AWG, 15.9 mm
L3	0.679 $\mu$ H	7 turns, 20 AWG, 9.652 mm	7 turns, 10 AWG, 14 mm

In order to fabricate the PCB for the circuit, the layout tool of ADS was used. At first, some doubts appeared of what substrate to use. Based on the microstrips width, it was possible to choose the most appropriate one.

The first considered was the RT/duroid® 5880 from Rogers Corporation. At LineCalc, a microstrip calculation

tool of ADS, the following parameters that described the substrate were inserted:

$$\begin{aligned}
 \epsilon_r &= 2.2, \\
 \mu_r &= 1, \\
 H &= 3.18 \text{ mm}, \\
 Hu &= 3.9e + 34, \\
 T &= 35\mu\text{m}, \\
 Cond &= 5.8e7, \\
 \tan \delta &= 0.0004, \\
 Freq &= 13.6 \text{ MHz}, \\
 Z_0 &= 50 \Omega, \\
 E_{eff} &= 10^\circ.
 \end{aligned}$$

The output was:

$$\begin{aligned}
 W &= 9.734940, \\
 L &= 446.677000.
 \end{aligned}$$

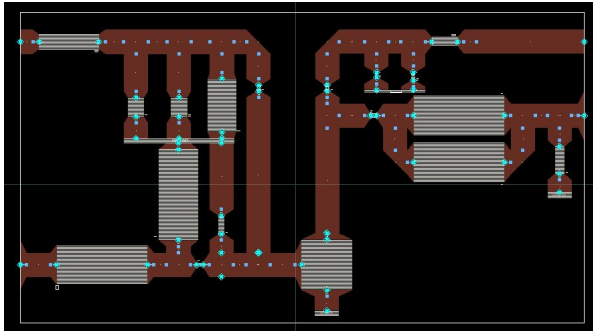
Then, testing the same thing for the FR-4 substrate, the following parameters were inserted:

$$\begin{aligned}
 \epsilon_r &= 4.6, \\
 \mu_r &= 1, \\
 H &= 1.6 \text{ mm}, \\
 Hu &= 3.9e + 34, \\
 T &= 35\mu\text{m}, \\
 Cond &= 5.8e7, \\
 \tan \delta &= 0.018, \\
 Freq &= 13.6 \text{ MHz}, \\
 Z_0 &= 50\Omega, \\
 E_{eff} &= 10^\circ.
 \end{aligned}$$

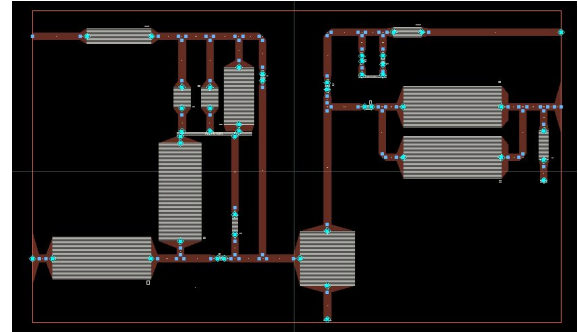
The output was:

$$\begin{aligned}
 W &= 2.810500, \\
 L &= 324.289000.
 \end{aligned}$$

Since a much smaller width ( $W$ ) was obtained with the FR-4 substrate, at 13.6 MHz, this was the one chosen for this project. It is important to emphasize that the length ( $L$ ) is not very relevant in this choice, since it can be easily modified by the electric length ( $E_{eff}$ ), which is only rotating in the Smith Chart. By choosing the FR-4, it was possible to optimize the circuit dimensions from  $226.3 \times 124.8$  mm (5880) to  $196.54 \times 116.10$  mm (FR-4). In Figure 45, it shows a comparison between these two layouts, one with Rogers RT/duroid® 5880 and the other with FR-4.



(a) Circuit using RT/duroid® 5880



(b) Circuit using FR-4

Figure 45: Comparison between two substrates

In Figure 46, there is the final version of the layout, where the right side was rotated and mirrored and the squares that represent the lumped components were removed.

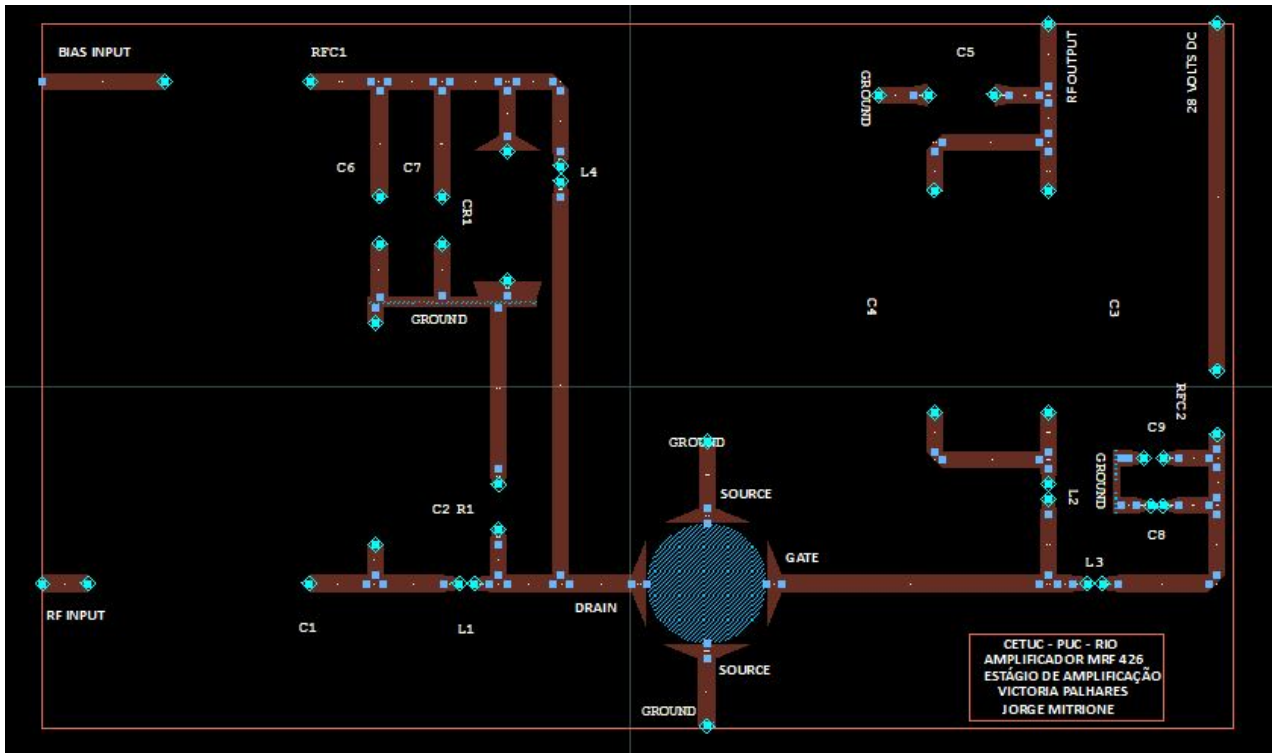


Figure 46: Final Layout for the MRF 426 in FR-4

## 4.b.2. Simulation

After thinking about the circuit design, the decision was to simulate in order to align the expectations for the experiments.

In Figure 47, the schematic used in the simulation is shown.

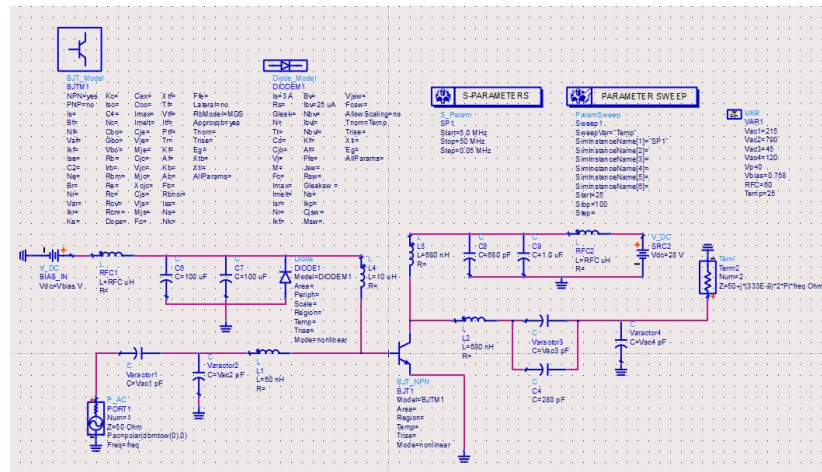


Figure 47: Simulation Schematic in ADS

The obtained results of the simulation from 5 to 50 MHz are shown in Figure 48 and 49. In Figure 48, the parameter S21 (transmitted wave in Port 2 given an incident wave in Port 1) was converted to power and in Figure 49 this previous curve was converted into dB.

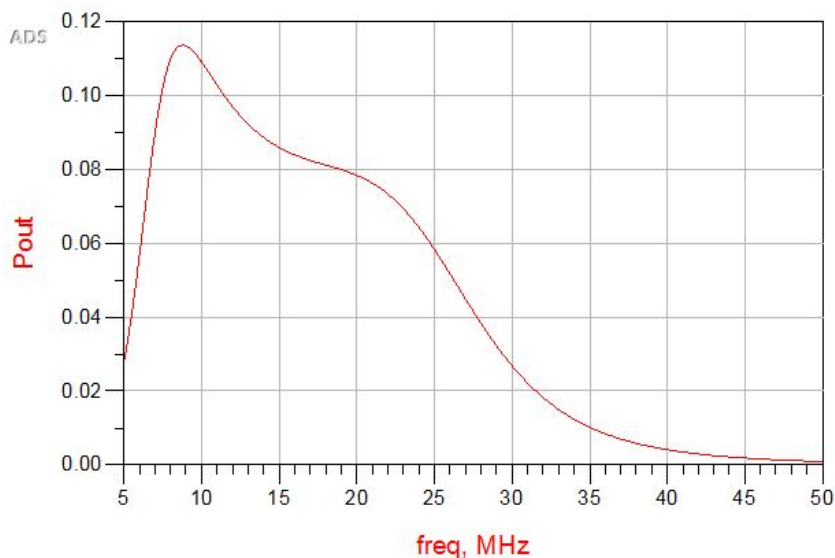


Figure 48: Power from S21(Transmitted Power)

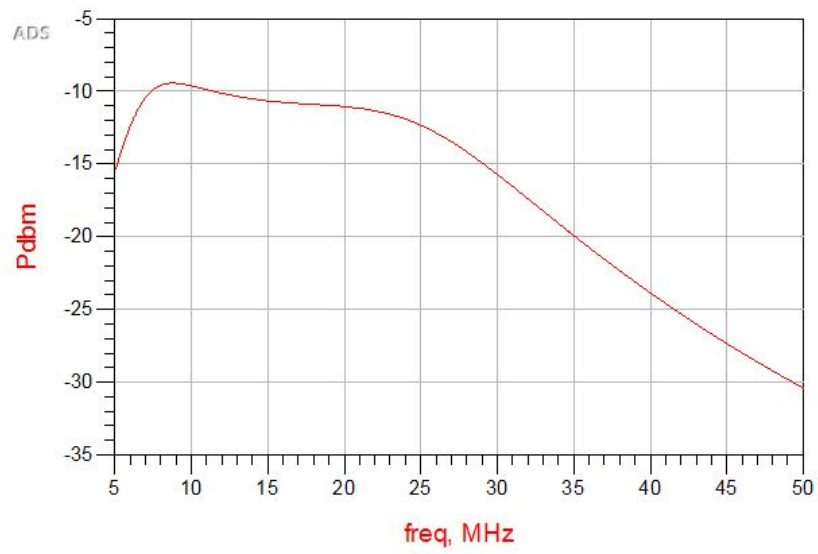


Figure 49: Transmitted Power in dB

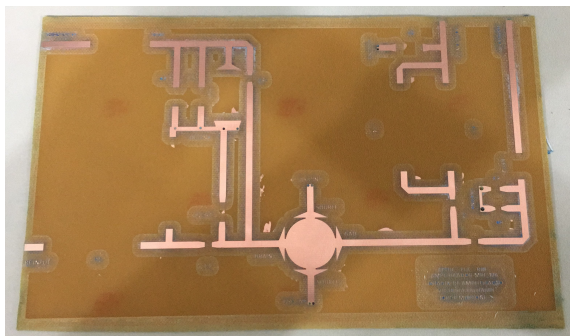
#### 4.b.3. Fabrication

After the layout has been made, it was exported from ADS as a gerber file in order to fabricate the circuit. The machine used was the LPKF ProtoMat S103 (Figure 50), a circuit board plotter configured specifically for RF and microwave requirements [9]. To turn the gerber file into instructions for the machine, the software CircuitPro was used, turning layout data into instructions for the PCB plotter [29]. Both LPKF ProtoMat S103 and Circuit Pro are from LPKF Laser & Electronics.

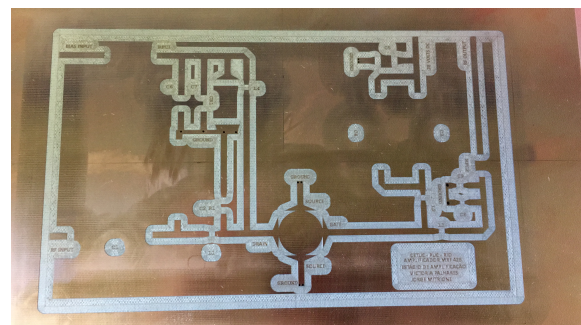


Figure 50: LPKF ProtoMat S103 [9]

Since this is a prototype, the decision was to plot two boards, being both fabricated by the LPKF ProtoMat. The plotter does not extract the conductor in all the desired area, so the option was to use ferric chloride in one of them to properly extract the conductor to obtain the desired circuit. In Figure 51, both boards are shown:



(a) Board 1 - Corroded by Ferric Chloride



(b) Board 2 - Without Corrosion

Figure 51: Two Prototypes - With and without Ferric Chloride

After having these two boards ready, the one corroded by the ferric chloride was used to start soldering the components. In Figure 52, the decision was not to fix the capacitors in the board, so that they could be easily taken out if necessary. To ground the circuit, epoxy paste was used. Even so, during one of the experiments, the isolation burned. Then, all the epoxy was changed by bolts linking the microstrip to the ground plane.

In Figure 52, the final PCB is shown:

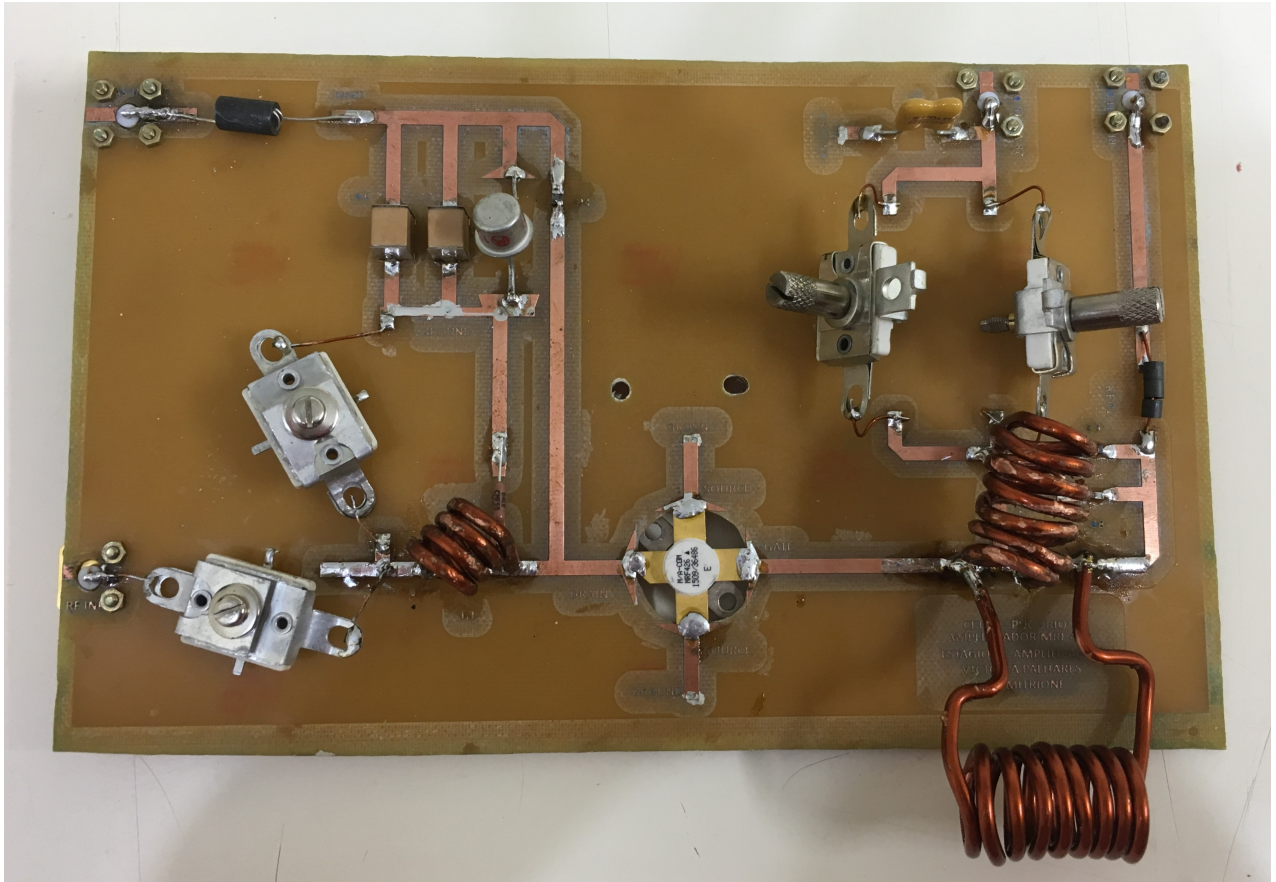


Figure 52: Final Circuit

During a few experiments, the  $10\ \Omega$  resistance was removed due to a short circuit appearing at the base. After a few experiments, it was noticeable that the epoxy paste was not properly grounding the circuit, causing the short circuit. Then, after solving this, the resistance was put back in its place. As a result, the original schematic from the datasheet was maintained in the final version of the circuit.

## 5. Experiments

### 5.a. Experimental Protocol

#### 5.a.1. Vector Network Analyzer (VNA)

A VNA is an instrument that enables the RF performance of RF and microwave devices to be characterized in terms of network parameters. In this work, the VNA was used not only to measure scattering parameters (S-parameters) in amplitude and phase, but also to measure incident power and transmitted power in dB. This equipment can be also used to measure other network parameters sets such as Y-parameters, Z-parameters and H-parameters. They are usually used to characterized two-port network devices, but can also measure an arbitrary number of port devices, when the other ports are load matched.

The VNA used in this work was the Hewlett Packard 8714ET RF Network Analyzer/ 300kHz - 3000MHz, with maximum output power of +20 dBm.

In Figure 53, it is shown the VNA model used in this project.



Figure 53: VNA

### 5.b. Configuration 1: Just the PA

First, experiments were made with the PA by itself. In Figure 54, there is an schematic of this experiment. In this case, it was extremely important to properly isolate the VNA so that there was not a reflected wave at the PA's port 1 (S11) that could damage the source (VNA).

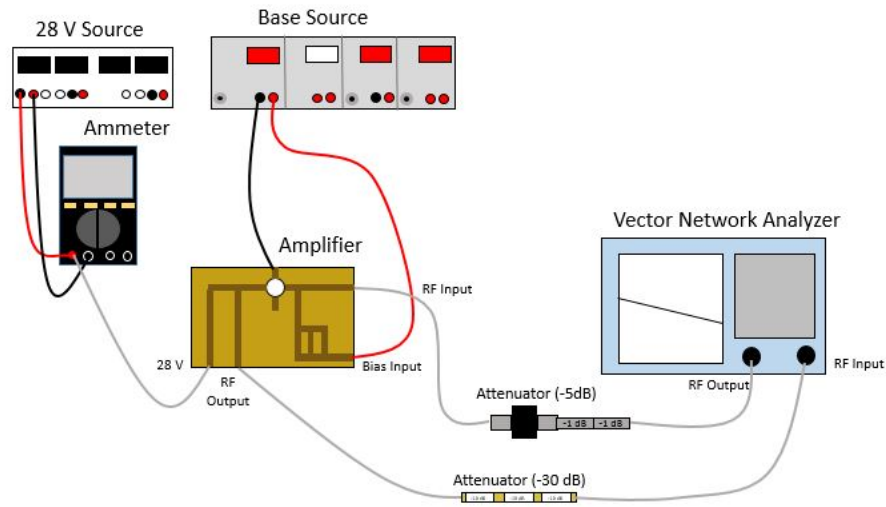


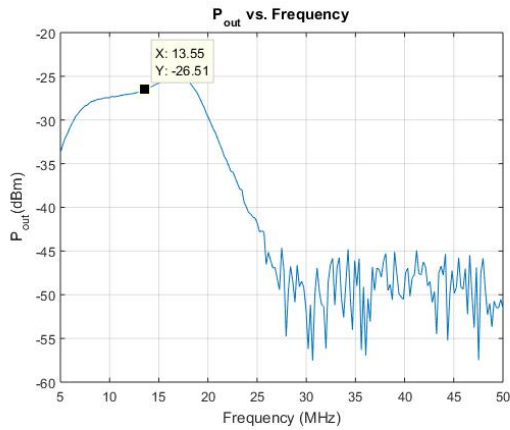
Figure 54: PA Test

In Figure 55, the attenuators used in this experiment are shown.

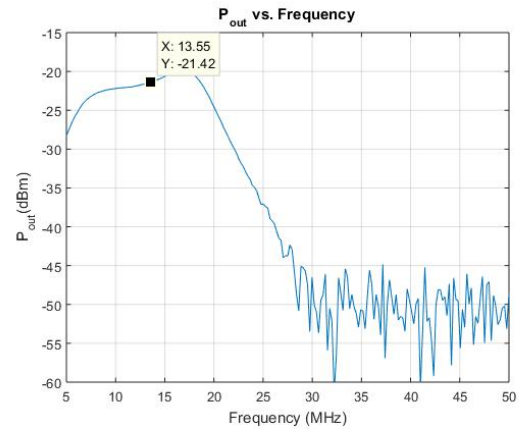


Figure 55: Circuit Attenuators

By varying the output power from -10 dBm to +16 dBm, it was possible to obtain the curves shown below from Figure 56 to 60.

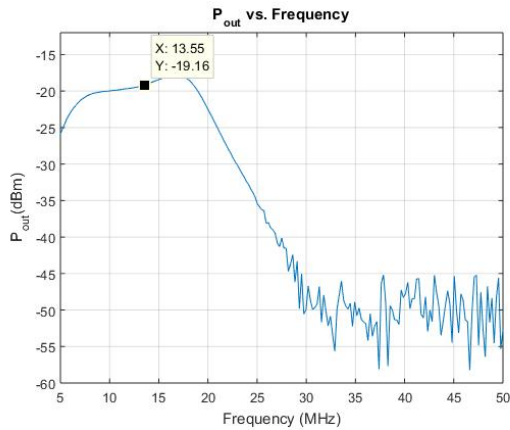


(1) Source : -10 dBm,  $I_C = 34 \text{ mA}$

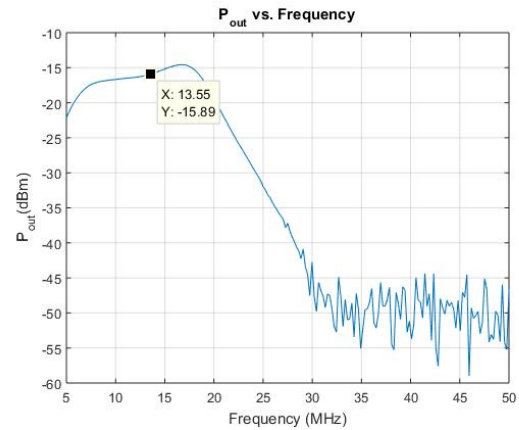


(2) Source : -5 dBm,  $I_C = 37.5 \text{ mA}$

Figure 56: Output power when input power is -10 dBm and -5 dBm

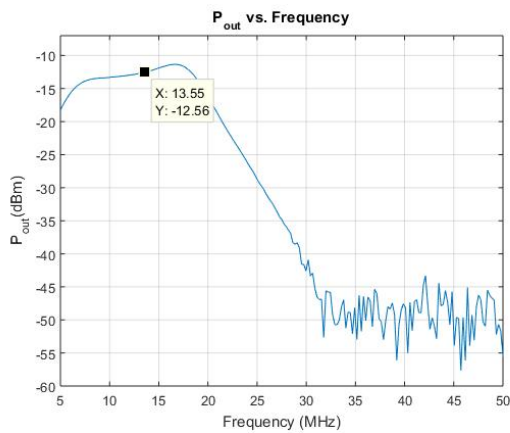


(3) Source : -3 dBm,  $I_C = 42 \text{ mA}$

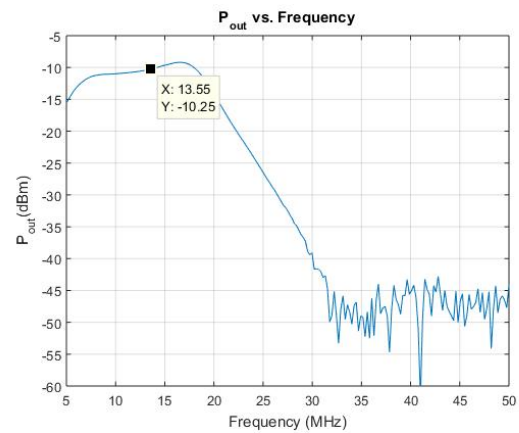


(4) Source : 0 dBm,  $I_C = 45 \text{ mA}$

Figure 57: Output power when input power is -3 dBm and 0 dBm

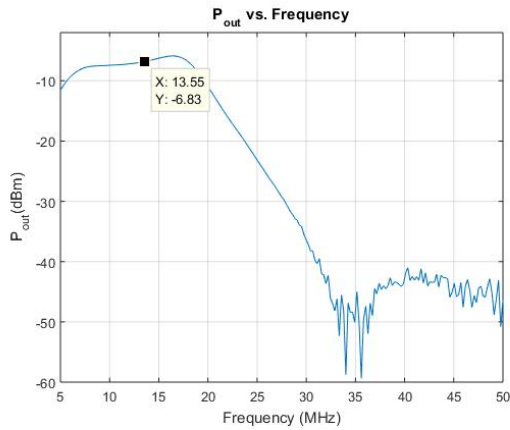


(5) Source : 3 dBm,  $I_C = 53.5 \text{ mA}$

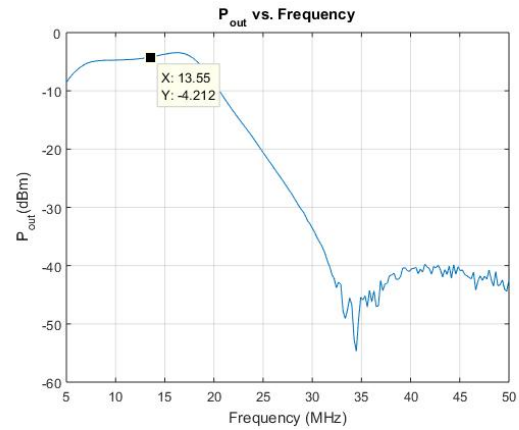


(6) Source : 5 dBm,  $I_C = 60.5 \text{ mA}$

Figure 58: Output power when input power is 3 dBm and 5 dBm

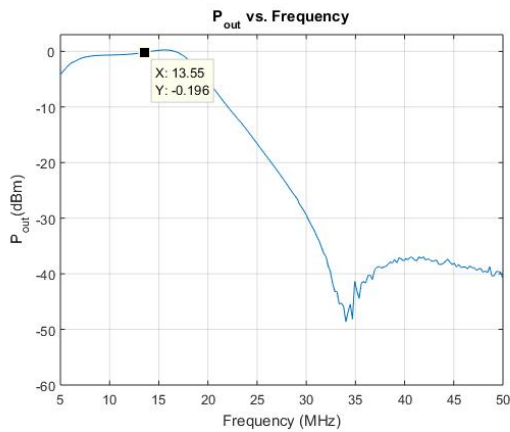


(7) Source : 8 dBm,  $I_C = 79 \text{ mA}$

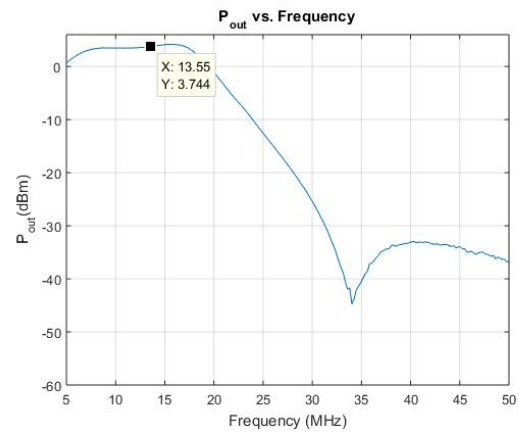


(8) Source : 10 dBm,  $I_C = 100 \text{ mA}$

Figure 59: Output power when input power is 8 dBm and 10 dBm



(9) Source : 13 dBm,  $I_C = 200 \text{ mA}$



(10) Source : 16 dBm,  $I_C = 230 \text{ mA}$

Figure 60: Output power when input power is 13 dBm and 16 dBm

In the figures above, each time that the VNA output power was increased, there was an increment in the BJT collector's current. Additionally, it was possible to observe that every increment in the VNA output power corresponds to a proportional increment in the PA output power, showing that the gain is approximately the same and independent from the PA RF input. In Table 7, it is shown the stability of the gain around 20 dB .

Table 7: Results - PA Experiment

Input (dBm)	Output (dBm)	Gain (dB)
- 10	-26.51	21.49
- 5	-21.42	18.58
- 3	-19.16	18.84
0	-15.89	19.11
3	-12.58	19.42
5	-10.25	19.75
8	-6.83	20.17
10	-4.212	20.78
13	-0.196	21.80
16	3.744	22.744

## 5.c. Configuration 2: Using MTM with the PA

### 5.c.1. Lightning up a LED

For the following experiments the DC sources and the ammeter were kept and the attenuators were removed. This time, the protection of the VNA is still necessary but without compromising the power supply, which is now, fixed in +16 dBm. Therefore, the 35 dB attenuation was replaced to a 6 dB between VNA and the PA input (Figure 61). Additionally, the PA output was connected to a transmitter coil in order to transmit wireless power to a receiver coil connected to a rectifier circuit with a LED. The objective this time was to measure the maximum distance between transmitter and receiver coil to light up the LED. Then, by adding 1 or 2 slabs of MTM, the desire was to increase this distance. In Figure 62 and 63, a schematics of the experiments can be seen, first with MTM 1 (13.6 MHz) and then with MTM 2 (33 MHz). By varying the position of the slab between coils, it was possible to see different results.

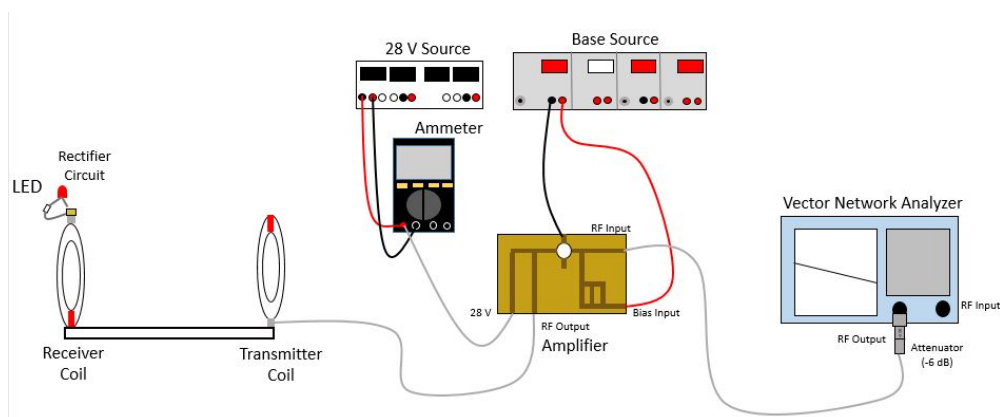
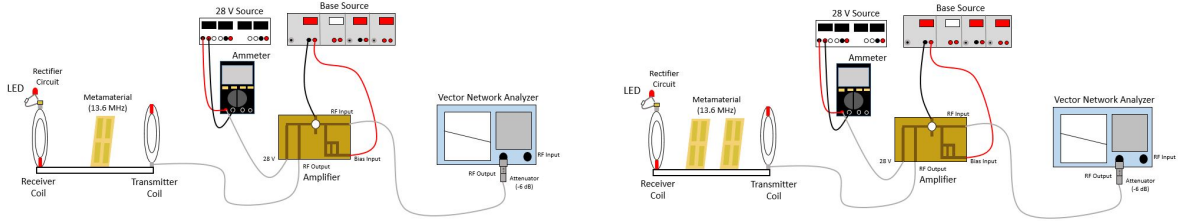


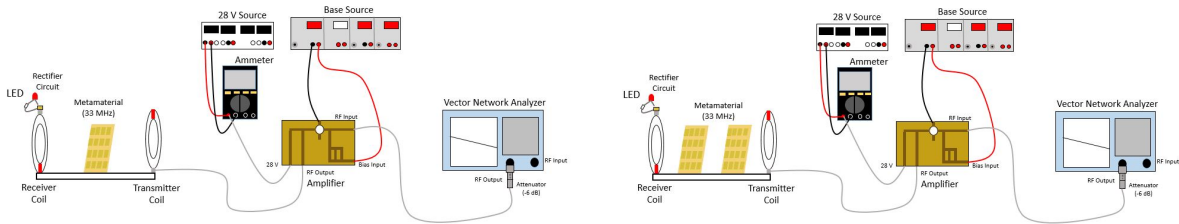
Figure 61: Experiment without MTMs



(a) One Slab of MTM 1 (13.6 MHz)

(b) Two Slabs of MTM 1 (13.6 MHz)

Figure 62: Experiment with MTM 1 (13.6 MHz)



(a) One Slab of MTM 2 (33 MHz)

(b) Two Slabs of MTM 2 (33 MHz)

Figure 63: Experiment with MTM 2 (33 MHz)

In Figure 64, the inductive coupling coils and the attenuator used in the experiment are presented.



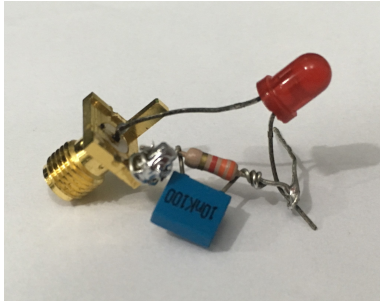
(a) Inductive Coupling Coils



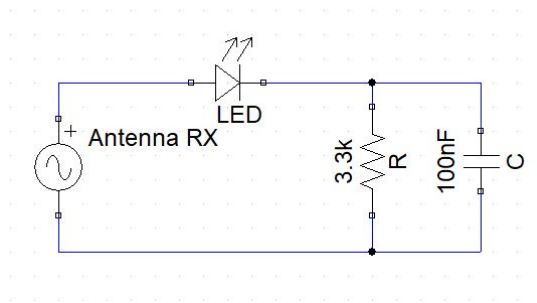
(b) 6 dB Attenuator

Figure 64: Equipment used in the experiment

In Figure 65, the rectifier circuit used together with its schematic is presented.



(a) Rectifier Circuit



(b) Schematic of the circuit

Figure 65: Rectifier Circuit

In Table 8, the results obtained through this experiment are shown.

Table 8: LED Experiment

Experiment	Distance (Transmitter and Receiver)	Distance (MTM and Transmitter)	Distance (MTM and Receiver)
No MTM	5.3 cm	N/A	N/A
One MTM 1 (13.6 MHz)	6.35 cm	1 cm	5.35 cm
One MTM 2 (33 MHz)	5.5 cm	1 cm	4.5 cm
One MTM 1 (13.6 MHz)	7.8 cm	7.3 cm	0.5 cm
One MTM 2 (33 MHz)	6.53 cm	6.27 cm	0.26 cm
One MTM 1 (13.6 MHz)	6.5 cm	3.29 cm	2.8 cm
One MTM 2 (33 MHz)	7 cm	3.45 cm	3.45 cm
Two MTMs 1 (13.6 MHz)	11.09 cm	0.58 cm	0.89 cm
Two MTMs 2 (33 MHz)	7.35 cm	1.1 cm	0.6 cm

## 5.c.2. Measuring Power

In this last experiment, the previous one was reproduced, but now, instead of the rectifier circuit with the LED, the receiver coil was connected back to the VNA in order to measure the power received by the LED and have precise results. In Figure 66, 67 and 68, a schematic of this last experiment is shown. To correctly obtain the power received by the LED, the same distances obtained in the last experiment were used.

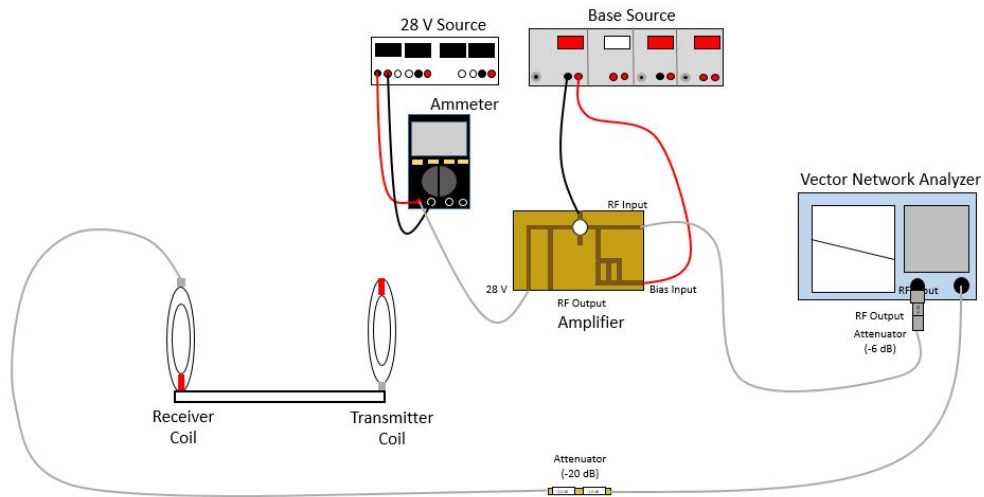
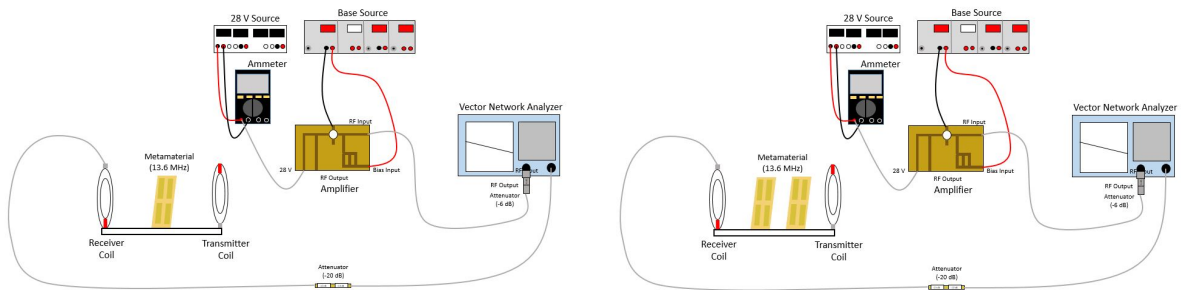


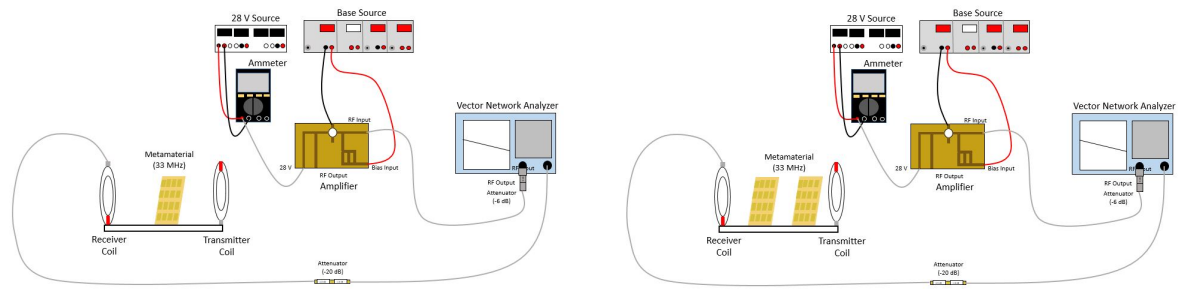
Figure 66: Experiment without MTMs



(a) One Slab of MTM 1 (13.6 MHz)

(b) Two Slabs of MTM 1 (13.6 MHz)

Figure 67: Experiment with MTM 1 (13.6 MHz)



(a) One Slab of MTM 2 (33 MHz)

(b) Two Slabs of MTM 2 (33 MHz)

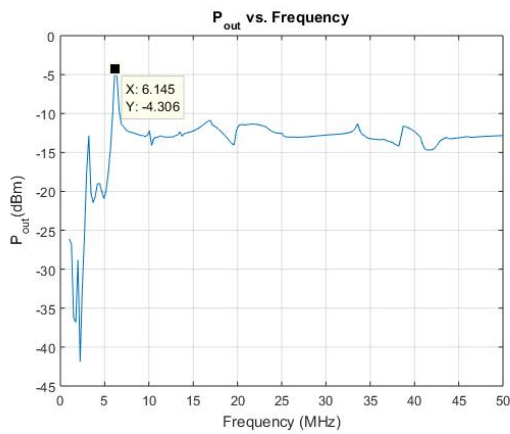
Figure 68: Experiment with MTM 2 (33 MHz)

In order to not damage the VNA with the power received by the coil, a 20 dB attenuator was used between receiver coil and VNA (Figure 69).

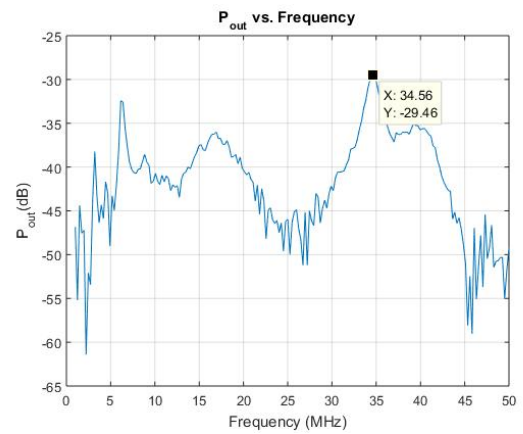


Figure 69: 20 dB Attenuator

The obtained graphics are shown in Figure 70 to 74 :

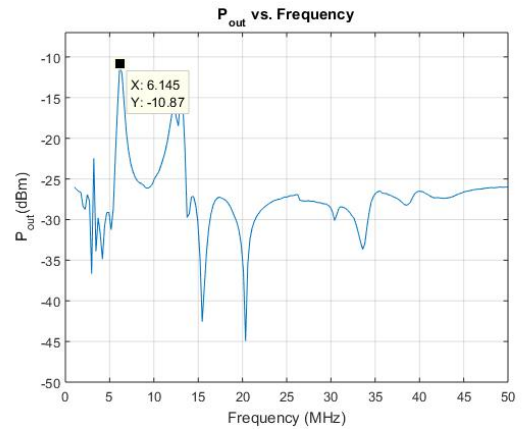
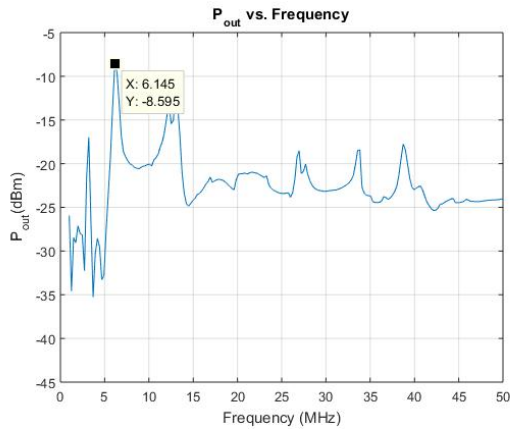


(a) Without MTM



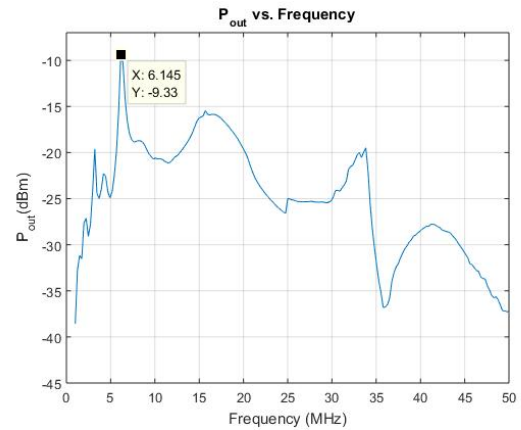
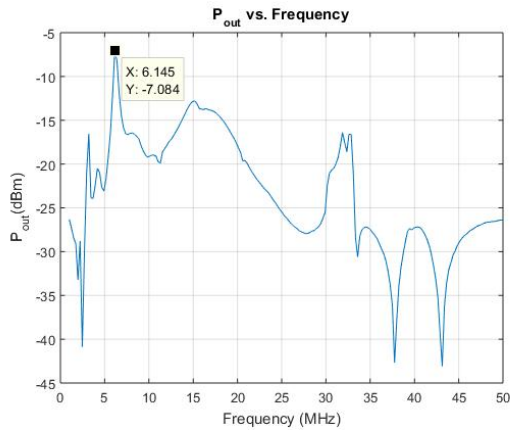
(b) Metal board blocking the link

Figure 70: Without MTM



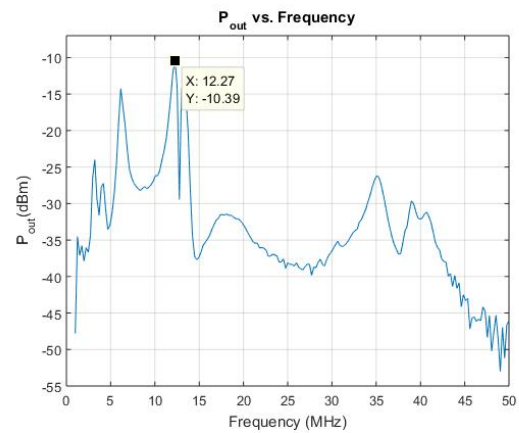
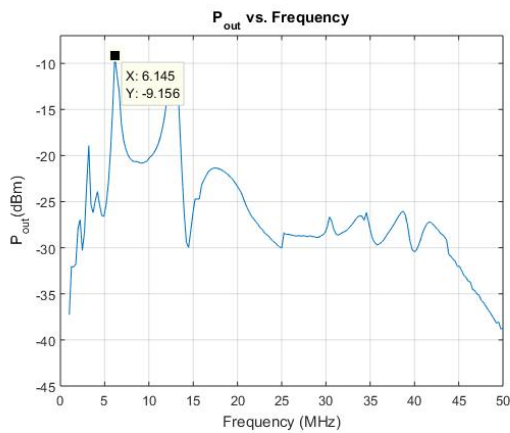
(a) One Slab of MTM 1 (13.6 MHz) assisting the Transmitter      (b) One Slab of MTM 1 (13.6 MHz) assisting the Receiver

Figure 71: One Slab of MTM 1 (13.6 MHz) assisting the Transmitter and the Receiver



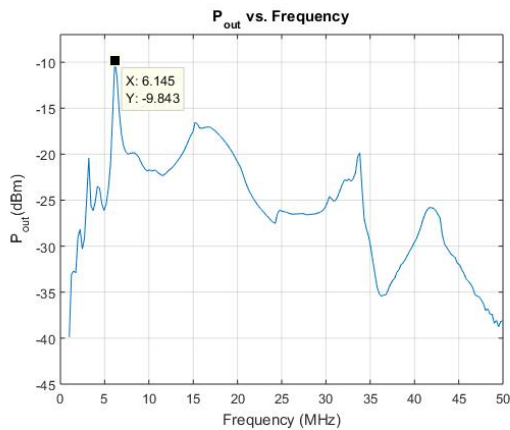
(a) One Slab of MTM 2 (33 MHz) assisting the Transmitter      (b) One Slab of MTM 2 (33 MHz) assisting the Receiver

Figure 72: One Slab of MTM 2 (33 MHz) assisting the Transmitter and the Receiver

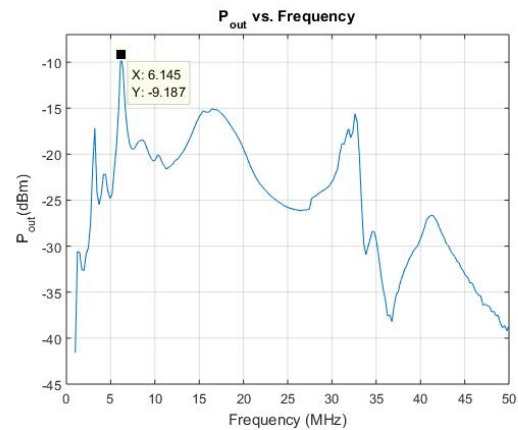


(a) One Slab of MTM 1 (13.6 MHz) between the Transmitter and the Receiver      (b) Two Slabs of MTM 1 (13.6 MHz) one assisting the Transmitter and the other assisting the Receiver

Figure 73: Two experiments with MTM 1 (13.6 MHz)



(a) One Slab of MTM 2 (33 MHz) between the Transmitter and the Receiver



(b) Two Slabs of MTM 2 (33 MHz) one assisting the Transmitter and the other assisting the Receiver

Figure 74: Two experiments with MTM 2 (33 MHz)

Through these experiments, it was possible to observe the increment in distance when adding one MTM slab and two. Even though the best case happens with an addition of two slabs, when assisting the receiver coil with one MTM slab, it was possible to achieve greater distances than when assisting the transmitter coil. Furthermore, in all the experiments a frequency shift was observed due to the imperfections in the MTM slabs. It is noticeable that in the majority of the cases, the maximum power could be seen at 6.14 MHz. Nevertheless, an amplification could still be seen with the addition of MTM.

## 6. Conclusions

### 6.a. Main Results

The main conclusions taken from this project and experiments are:

- The PA achieved stable gain, independent from its RF input.
- In order to build a PA connected to a very reactive load, its BJT needs to be carefully chosen (high VSWR) in order to not cause a reflected wave back to the circuit and consequently, damage it.
- When operating with one MTM slab, 13.6 and 33 MHz, it is more efficient to position it close to the receiver coil.
- Both 13.6 MHz and 33 MHz MTM slabs are more efficient working in pairs.
- When working in pairs, the efficiency is independent from the position of the MTM slabs, for 13.6 and 33 MHz. As a result, transmitters and receivers can be designed as compact as possible, without decreasing the efficiency of the link.
- When adding one or two MTM slabs, a frequency shift is observed.

### 6.b. Future Work

In this project, there was not enough time to conduct all the experiments desired and to sophisticate the PA system.

Other future progresses aimed for this work are:

- Same experiments with the MTM slabs misaligned.
- Experiment fixing the distances found in Section 5.c.2 and varying the position of the MTM slab in 10 parts, from the transmitter to the receiver coil. Proposed for both types of MTM.
- Experiment fixing the distances found in Section 5.c.2 and monitoring the temperature of the MTM slabs every 5 minutes in order to observe changes in the system behaviour after some time. Proposed for both types of MTM.
- Design a oscillating circuit to connect to the PA in order to create a sinusoidal independent source. By this, an independent source of wireless power could be created.

## References

- [1] J. V. de Almeida, "Metamaterials applied to inductive wireless power transmission," Bachelor's Thesis, Pontifical Catholic University of Rio de Janeiro, Brazil, June 2015.
- [2] R. N. A. M. Vikram Iyer, Elyas Bayati and S. Gollakota, "Charging a Smartphone Across a Room Using Lasers." *Interactive, Mobile, Wearable and Ubiquitous Technologies*, vol. Vol. 1, No. 4, Article 143, 2017.
- [3] J. B. P. D. R. Smith and M. C. K. Wiltshire, "Metamaterials and negative refractive index." *Science*, vol. 305, 2004.
- [4] E. C. Silva, "Analog electronics," 4 2018, lecturer notes.
- [5] K. C. S. A. S. Sedra, *Microelectronics*. Oxford University Press, Inc., 2007.
- [6] W. H. K. Y. Lu, *CMOS Integrated Circuit Design for Wireless Power Transfer*. Springer, 2018.
- [7] A. C. Kubrusly, "Microwave devices," 6 2018, lecture notes.
- [8] *MRF426 - The RF Line NPN Silicon Power Transistor*, 2nd ed., M/A-COM Technology Solutions Inc., 100 Chelmsford Street, Lowell, MA 01851, United States.
- [9] LpKF protomat s103. [Online]. Available: <https://www.lpKF.com/products/rapid-pcb-prototyping/circuit-board-plotter/protomat-s103.htm>
- [10] H. J. Visser, "A Brief History of Radiative Wireless Power Transfer." *2017 11th European Conference on Antennas and Propagation (EUCAP)*, 2017.
- [11] Y. T. H. L. Xie, Y. Shi and A. Lou, "Wireless power transfer and applications to sensor networks." *IEEE Wireless Communications*, vol. 20, 2013.
- [12] A brief history of the qi specification. [Online]. Available: <https://www.wirelesspowerconsortium.com/developers/specification.html>
- [13] M. Moon. Apple acquires wireless charging company powerbyproxi. [Online]. Available: <https://www.engadget.com/2017/10/25/apple-wireless-charging-powerbyproxi/>
- [14] M. Chabalko, M. Shahmohammadi, and A. Sample. Quasistatic cavity resonance for ubiquitous wireless power transfer. [Online]. Available: <https://www.disneyresearch.com/publication/quasistatic-cavity-resonance-for-ubiquitous-wireless-power-transfer/>
- [15] R. M. J. D. J. P. F. M. S. André Kurs, Aristeidis Karalis, "Wireless Power Transfer via Strongly Coupled Magnetic Resonances." *Science*, vol. 317, 2007.
- [16] P. Fisher, R. Moffatt, M. Soljačić, A. Kurs, J. Joannopoulos, and A. Karalis. Our story. [Online]. Available: <http://witricity.com/company/our-story/>
- [17] M. Golden and M. Shwartz. Wireless charging of moving electric vehicles overcomes major hurdle in new stanford research. [Online]. Available: <https://news.stanford.edu/2017/06/14/big-advance-wireless-charging-moving-electric-cars/>
- [18] P. Y. M. G. M. Kiani, B. Lee, "A Q-Modulation Technique for Efficient Inductive Power Transmission." *IEEE J Solid-State Circuits*, vol. 2839–2848, 2015.
- [19] P. C. K. L. S. Aldhaher, "Wireless Power Transfer Using Class E Inverter with Saturable DC-Feed Inductor." *IEEE Transactions on Industry Applications*, vol. Volume 50, Issue 4, Pages 2710-2718, 2014.
- [20] C. A. Balanis, *Antenna Theory*. John Wiley & Sons, Inc., 1997.
- [21] S. M. Wentworth, *Fundamentals of Electromagnetics with Engineering Applications*. LTC, 2006.
- [22] J. B. Pendry, "Negative refraction makes a perfect lens." *Phys Rev Lett*, vol. vol. 85, 2000.
- [23] A. T. F. Bilotti and L. Vegni, "Design of Spiral and Multiple Split-Ring Resonators for the Realization of Miniaturized Metamaterial Samples." *IEEE TRANSACTIONS ON ANTENNAS AND PROPAGATION*, vol. vol. 55, no. 8, pp. 2258-2265, 2007.
- [24] C. M. S. C. Amaral, "Near field lenses based on metamaterials for rfid antennas," Bachelor's Thesis, Pontifical Catholic University of Rio de Janeiro, Brazil, 12 2017.
- [25] Amplifier classes. [Online]. Available: <https://www.electronics-tutorials.ws/amplifier/amplifier-classes.html>
- [26] Class c amplifier. [Online]. Available: <http://home.sandiego.edu/~ekim/e194rfs01/lec24ek.pdf>

- [27] Advanced design system (ads). [Online]. Available: <https://www.keysight.com/en/pc-1297113/advanced-design-system-ads?cc=BR&lc=por>
- [28] Coil inductance calculator. [Online]. Available: <https://www.allaboutcircuits.com/tools/coil-inductance-calculator/>
- [29] Lpkf circuitpro pm. [Online]. Available: <https://www.lpkf.com/products/rapid-pcb-prototyping/software/circuitpro-pm.htm>